

**EXPERIMENTAL AND NUMERICAL ANALYSIS OF ENVIRONMENTAL
CONTROL SYSTEMS FOR RESILIENT EXTRA-TERRESTRIAL
HABITATS**

by

Hunter A. Sakiewicz

A Thesis

Submitted to the Faculty of Purdue University

In Partial Fulfillment of the Requirements for the degree of

Master of Science in Mechanical Engineering



School of Mechanical Engineering

West Lafayette, Indiana

May 2023

**THE PURDUE UNIVERSITY GRADUATE SCHOOL
STATEMENT OF COMMITTEE APPROVAL**

Dr. Davide Ziviani, Chair

School of Mechanical Engineering

Dr. Ilias Bilonis

School of Mechanical Engineering

Dr. Shirley Dyke

School of Mechanical Engineering

Approved by:

Dr. Nicole L. Key

*Dedicated to my parents, Marty and Gina.
For their unconditional love and support.*

ACKNOWLEDGMENTS

This work is funded by NASA under grant or cooperative agreement award number 80NSSC19K1076.

Thank you, Professor Ziviani, for your guidance and support throughout this project. I appreciated your availability to meet and help me when I needed it despite your extremely busy schedule. Lastly, thank you for taking me under your wing when I was looking for an undergraduate research position. That experience helped me to decide to pursue graduate school and land a career in the HVAC industry.

I would also like to thank all of the great people at Herrick. Steven, thank you for being a great mentor. You helped me learn how to run psychrometric chambers, conduct experiments, and understand advanced HVAC technology. Abd, Weigang, Andreas, Parveen, thank you for helping me during my modeling efforts, analyzing data, and being available to answer all of the questions I had.

Frank and Jose, thank you for making sure that everything went smoothly with the heat pump. Christian, thank you for helping me understand data acquisition, sensors, and making sure everything went smoothly when I was running experiments.

Last but not least I would like to thank my mom, dad and Meredith for not only your love and support but also your help. Dad, given your 30+ years of experience in HVAC, thank you for answering my questions and helping me over the phone when problems arose. Meredith, your expertise in computers and networking helped me when I was having trouble with setting up the network to communicate with the heat pump remotely.

TABLE OF CONTENTS

LIST OF FIGURES	8
NOMENCLATURE	10
ABSTRACT.....	12
1. INTRODUCTION.....	13
1.1 Motivation.....	13
1.2 Resilient Extra-Terrestrial Habitat Institute.....	13
1.3 Cyber-Physical Testbed Description.....	14
1.4 Literature Review.....	16
1.5 Thesis Objectives and Approach	17
2. MODEL METHODOLOGY	18
2.1 Motivation.....	18
2.1.1 Literature Review.....	18
2.1.2 Heat Pump Modeling Inspiration.....	19
2.2 Heat Pump Cycle Model.....	20
2.2.1 Evaporator Model	23
2.2.2 Compressor Model.....	24
2.2.3 Condenser Model	27
2.2.4 Expansion Valve Model.....	27
2.2.5 Fan Model	28
3. CYBER-PHYSICAL TESTBED THERMAL MANAGEMENT SYSTEM.....	29
3.1 Experimental Setup.....	29
3.1.1 Data Acquisition Setup	30
3.1.2 Modbus Control Setup	33
3.2 Heat Pump Control Simulink Model	34
3.3 Heat Pump Data Acquisition Simulink Model	36
3.4 Heat Pump Experimental Procedure	38
3.4.1 Preliminary Experimentation	38
3.4.2 Model Validation Experiments.....	39
4. RESULTS AND MODEL VALIDATION	42

4.1	Motivation.....	42
4.2	Results.....	42
4.2.1	No-Load Experimental Results.....	42
4.2.2	Cooling Load Results.....	46
4.2.3	Heating Load Results.....	53
4.3	Discussion.....	59
4.4	Model Validation.....	60
5.	PARAMETRIC STUDY.....	62
5.1	Motivation.....	62
5.2	No Disturbance Load Calculations.....	62
5.3	Thermal Transfer Panel Load Calculations.....	66
5.4	Results and Discussion.....	66
6.	CONCLUSIONS AND FUTURE WORK.....	75
	APPENDIX. MINI-SPLIT OPERATING PROCEDURE.....	77
	REFERENCES.....	78

LIST OF TABLES

Table 1: Geometrical parameters in evaporator model.....	24
Table 2: Compressor Mapping coefficients	26
Table 3: Geometrical parameters in condenser model.....	27
Table 4: List of Sensors with Specifications and Tolerances	32
Table 5: Preliminary Experimental Test Plan.....	39
Table 6: Cooling Model Validation Experimental Test Plan.....	41
Table 7: Heating Model Validation Experimental Test Plan.....	41
Table 8: Sensible Cooling Load Test Metrics.....	49
Table 9: Sensible and Latent Cooling Load Test Metrics.....	53
Table 10: -40°C Panel Temperature Test Metrics	56
Table 11: -60 °C Panel Temperature Test Metrics	59
Table 12: Human Heat and Moisture Rates (Adapted from [30])	63
Table 13: Heat Rates by Electronic Devices (Adapted from [30]).....	63
Table 14: Regolith Thermophysical Properties (Adapted from [32]).....	63

LIST OF FIGURES

Figure 1: Cyber-physical flow diagram (Adapted from [5])	15
Figure 2: Meteorite impact scenario cyber-physical coupling [6]	16
Figure 3: Representation of Heating System Analyses.....	19
Figure 4: Four Component Vapor Compression Cycle with State Points	20
Figure 5: Structure for Information Flow of the Component Sub-Models.....	21
Figure 6: Heat Pump Cycle Solver Algorithm.....	22
Figure 7: Schematic of Evaporator Model Displaying Partially Wet/Partially Dry Analysis	23
Figure 8: Habitat Prototype Consisting of Geodesic Dome and Inflatable Bladder.....	29
Figure 9: Triangular Thermal Transfer Panel	30
Figure 10: Heat Pump Sensor Schematic.....	31
Figure 11: Experimental Setup with Wiring Schematic	31
Figure 12: Thermocouple Inputs to I/O Module.....	32
Figure 13: Sensor Inputs to Voltage I/O Module.....	33
Figure 14: Modbus Slave Gateway Connection Schematic.....	34
Figure 15: Setup and Connection Simulink Code.....	35
Figure 16: Writing a Holding Register Simulink Code	35
Figure 17: Heat Pump Control Panel	36
Figure 18: Screenshot of Simulink CPT Control Panel with Data Acquisition.....	37
Figure 19: Screenshot of m+p Dynamic Signal Analyzer	37
Figure 20: Schematic of Testbed During Model Validation Experimentation	40
Figure 21: No-Load Cooling Pressure and Temperature vs Time at Cycle State Points.....	43
Figure 22: Bladder Air Temperature vs Time Cooling Mode	43
Figure 23: No-Load Heating Pressure and Temperature vs Time at Cycle State Points.....	45
Figure 24: Bladder Air Temperature vs Time Heating Mode.....	45
Figure 25: Sensible Cooling Load Test Pressure and Temperature vs Time at Cycle State Points	47
Figure 26: P-h Diagram of Sensible Cooling Load Test at Steady State.....	47
Figure 27: Bladder Air Temperature vs Time Sensible Cooling Load Test.....	48

Figure 28: Sensible and Latent Cooling Load Test Pressure and Temperature vs Time at Cycle State Points.....	50
Figure 29: P-h Diagram of Sensible and Latent Cooling Load Test at Steady State.....	51
Figure 30: Bladder Air Temperature vs Time: Sensible and Latent Cooling Load Test.....	51
Figure 31: Bladder Relative Humidity vs Time: Sensible and Latent Cooling Load Test.....	52
Figure 32: -40°C Panel Temperature Test Pressure and Temperature vs Time at Cycle State Points	54
Figure 33: P-h Diagram of -40°C Panel Temperature Test at Steady State	54
Figure 34: Bladder Air Temperature vs Time -40°C Panel Temperature Test.....	55
Figure 35: -60°C Panel Temperature Test Pressure and Temperature vs Time at Cycle State Points	57
Figure 36: P-h Diagram of -60°C Panel Temperature Test at Steady State	57
Figure 37: Bladder Air Temperature vs Time -60°C Panel Temperature Test.....	58
Figure 38: Measured vs Predicted Evaporating Temperature (left) and Condensing Temperature (right)	60
Figure 39: Measured vs Predicted Capacity (left) and Power Consumption (right).....	61
Figure 40: Temperature at Various Depths of the Structural Protective Layer vs Time (Adapted from [32]).....	64
Figure 41: Load Profile Developed for Studying HVAC System Requirements and Response ..	65
Figure 42: Capacity as a Function of Evaporating and Condensing Temperature at Minimum Compressor Speed	67
Figure 43: Capacity as a Function of Evaporating and Condensing Temperature at Intermediate Compressor Speed	67
Figure 44: Capacity as a Function of Evaporating and Condensing Temperature at Rated Compressor Speed	68
Figure 45: Validation of IE Model Air Temperature vs Time.....	69
Figure 46: Load of 1227 W IE Air Temperature vs Time	70
Figure 47: Load of 2898 W IE Air Temperature vs Time	70
Figure 48: Load of -4330 W IE Air Temperature vs Time.....	71
Figure 49: Load of 7500 W IE Air Temperature vs Time	72
Figure 50: Load of -9000 W IE Air Temperature vs Time.....	72
Figure 51: Sensible Heat Ratio vs Pressure at Different Relative Humidities	73

NOMENCLATURE

Symbols:

c	Linear Regression Coefficient
h	Specific Enthalpy [kJ/kg]
Hz	Rotational Speed [1/s]
\dot{m}	Mass Flow Rate [kg/s]
Nu	Nusselt Number [-]
P	Pressure [Pa]
Pr	Prandtl Number [-]
\dot{Q}	Heat Transfer Rate [W]
Ra	Rayleigh Number [-]
T	Temperature [°C] or [K]
\dot{W}	Power Consumption [W]
η_s	Isentropic Efficiency [-]
ω	Humidity Ratio [kg/kg]

Acronyms:

API	Application Programming Interface
COP	Coefficient of Performance
CPT	Cyber-Physical Testbed
ECLSS	Environmental Control and Life Support System
EXV	Electronic Expansion Valve
HIL	Hardware-in-loop
HVAC	Heating, Ventilation, and Air Conditioning
IE	Interior Environment
MCVT	Modular Coupled Virtual Testbed
NASA	National Aeronautics and Space Administration
RETHi	Resilient Extra-Terrestrial Habitat Institute
RH	Relative Humidity
VCC	Vapor Compression Cycle

Subscripts:

cond	Condenser
comp	Compressor
ev	Expansion Valve
evap	Evaporator
s	Isentropic
SC	Subcooling
SH	Superheat
1,2,3,4	State Points

ABSTRACT

As space exploration continues to advance, so does the drive to inhabit celestial bodies. In order to expand our civilization to the Moon or even other planets requires an enormous amount of research and development. The Resilient Extra-Terrestrial Habitat Institute is a NASA funded project that aims to develop the technology needed to establish deep-space habitats. Deep-space inhabitation poses many challenges that are not present here on earth. The Moon, for example, has temperatures that range from -233 – 123°C . Aside from the extreme temperatures, a variety of thermal loads will need to be handled by the Environmental Control and Life Support System (ECLSS). Aside from the research and architecture of the International Space Station's ECLSS, very little information is known about disturbances related to the thermal management of extra-terrestrial habitats.

RETHi is developing a Cyber-Physical Testbed (CPT) that represents a one-fifth scale prototype of a deep space habitat. In order to answer difficult research questions regarding ECLSS and thermal management of a deep-space habitat, a heat pump was modeled and validated with the physical part of the CPT. Once validated, the heat pump model is able to accurately predict the steady state behavior given the indoor and outdoor conditions of the testbed. When coupled with the interior environment (IE) model, it gives insight into the system's requirements and response. Experimental testing was conducted with the heat pump in order to validate the model. After the model was validated, a series of parametric studies were conducted in order to investigate the effects of varying thermal loads and dehumidification. Since the groundwork was laid through model development and experimentation, future work consists of designing a more versatile heat pump to test a variety of disturbance scenarios. Although the heat pump model is specifically designed for the CPT, it proves to be versatile for other closed and pressurized environments such as aircraft and clean rooms according to the analysis of dehumidification and dependence on pressure.

1. INTRODUCTION

1.1 Motivation

Innately, humans are exploratory beings. Exploring allows for discovery and technological advancements. Exploration has allowed man to build a planet-spanning civilization. Looking up at the night sky made humans wonder what was up there. Soon enough they would not have to wonder anymore. The launch of Sputnik-I in 1957 initiated a space race and laid the foundation for space exploration. The space race continued and on July 20, 1969 Neil Armstrong had stepped foot where no man had ever stepped before: the Moon. Despite waning interests in manned lunar missions in the early 1970s, space exploration was far from over. Over the past six decades, quality of life on earth has improved due to space exploration. Without space programs we would not have global positioning systems, accurate weather predictions, advanced robotics, air purification systems, etc. Similarly, medical research is being conducted in space to cure diseases and prolong life. The possibilities and advancements are endless when it comes to space exploration.

Today, space is an avenue for business opportunities, technological advancements, and exploration of extraterrestrial habitats [1]. Many men and women have traveled to space but have yet to sustain long-term settlements. Putting it into perspective, Valeri Polyakov achieved the longest human spaceflight: 437 days. Upon returning, his first words were, “We can fly to Mars.” Since then, companies are developing technology for short-term and eventually long-term inhabitation on the Moon, Mars, and other celestial bodies [1]. As with any new endeavor, extraterrestrial habitation has many challenges. To this end, NASA has funded the Resilient Extra-Terrestrial Habitat Institute to conduct research towards deep-space inhabitation.

1.2 Resilient Extra-Terrestrial Habitat Institute

The Resilient Extra-Terrestrial Habitat Institute (RETHi) is a NASA-funded Space Technology Research Institute hosted at Purdue University and includes representatives from the University of Connecticut, Harvard University, and the University of Texas at San Antonio. In short, the goal of RETHi is to develop a smart autonomous habitat that is able to withstand deep-space disruptions without fundamental changes in function or sacrifices of safety [2]. Man has

created homes and other structures for thousands of years to meet their growing needs. The current need is a habitat that is able to withstand the harsh environments that the Moon and Mars have to offer. Unlike terrestrial habitats, deep-space habitats are subjected to extreme temperatures, dust storms, and meteoroid impacts. Due to the lack of resources and ability to send more supplies quickly, research must be conducted to develop the tools and techniques to support a resilient habitat. By taking what we already know about habitat construction coupled with next-generation technological advancements, we can overcome the deep-space habitation challenge.

The objective of this thesis in the context of RETHi is thermal and moisture management. The lunar diurnal cycle consists of 15 days of sunlight and 15 days of darkness. Temperatures during this cycle range from -233 – 123°C [3]. A deep-space habitat will have many thermal loads such as body heat and electronic cooling. Whether the habitat is manned or unmanned it is important to maintain a temperature similar to Earth for comfortability and electronics to function properly. Likewise, moisture inside the habitat is a concern. Almost all of the moisture in deep-space habitats comes from occupants via respiration or perspiration. It is important to maintain relative humidity of 40%-70% for proper health [4]. Relative humidity above 70% can lead to problems not only for the occupants but also the habitat. Humid conditions lead to dangerous microorganism growth, water condensate inside electronics, and inability to detect smoke. It is also worth noting that the ventilation rates of space habitat crew quarters are much higher than terrestrial buildings. The ventilation requirements for crew quarters is 0.42 - 5.1 m^3/min [5]. Conducting research of the temperature and humidity control will lead to the development of tools and techniques for resilience in the system.

1.3 Cyber-Physical Testbed Description

The Cyber-Physical Testbed (CPT) integrates physical testing with computer-based simulations to answer difficult research questions. The physical component comprises of prototypes that are novel and difficult to model whereas the computational component contains reliable and accurate models. These two partitions interact with each other via sensors and actuators. An appropriate transfer system enforces the boundary conditions of these two components [6]. Figure 1 shows a simplified cyber-physical testing architecture related to the topic of this work. By adopting this approach, research can be conducted to gain a further understanding

of the extreme environmental conditions experienced by deep-space habitats. In short, cyber-physical testing allows for experimentation that would otherwise be impossible or cost millions of dollars to run [6].

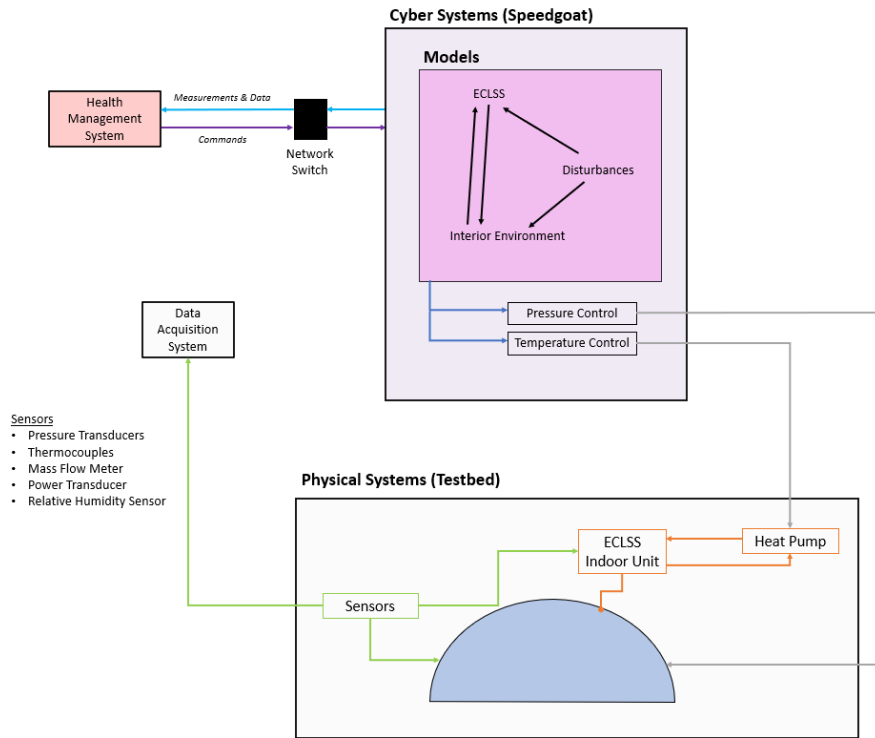


Figure 1: Cyber-physical flow diagram (Adapted from [6])

The physical parts of the testbed consist of an inflated bladder and structural dome which are surrounded by thermal transfer panels. The thermal transfer panels will later be controlled to impose an exterior thermal boundary condition similar to the lunar regolith protective layer experienced by deep-space habitats. To this end, cyber-physical testing plays a role in thermal management research. When a hazardous event presents itself such as a meteorite impact on the surface of the habitat, the lunar regolith protective layer is displaced causing a section of the habitat to be directly exposed to the lunar atmosphere [7]. This will result in temperature fluctuations within the interior environment (IE). The temperature control system will be responsible for managing this disruption. The cyber component will be the meteorite impact and resulting regolith layer model whereas the physical component will be a controllable temperature drop of the thermal transfer panel affected. Coupling these components together will allow researchers to gain insight

on how the thermal system is affected by a meteorite impact without actually damaging any real components. Figure 2 shows the coupling of cyber and physical components during a meteorite strike.

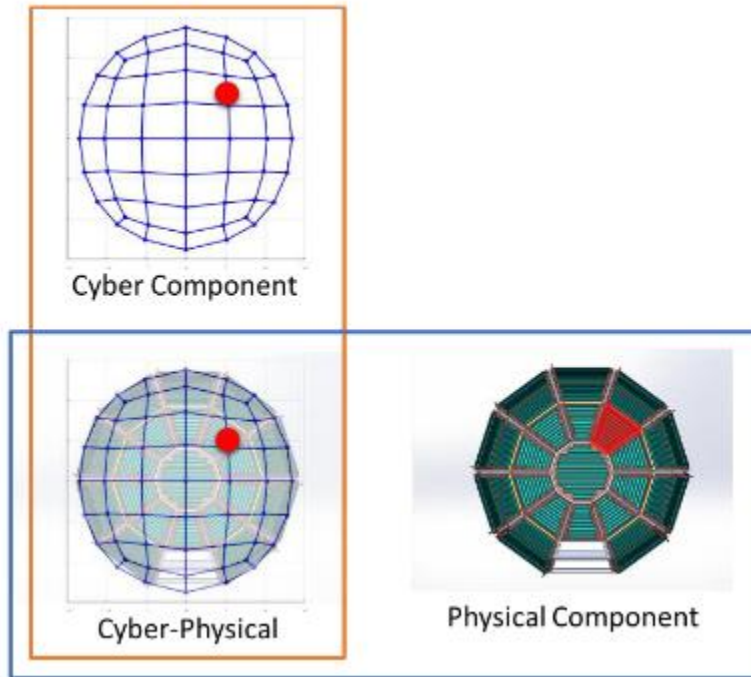


Figure 2: Meteorite impact scenario cyber-physical coupling [7]

1.4 Literature Review

RETHi is leading the field with groundbreaking research and developments related to extra-terrestrial inhabitation. Until today, there have been very few publications in open literature related to thermal and moisture management with respect to future habitats. Thermal control systems for Lunar and Martian exploration was studied as early as 1990 [8]. During this study, a heat pump was designed and theoretically analyzed for a Lunar habitat. In 1993, research done at The University of Arizona investigated heat pump architectures for low temperature heat rejection on Lunar bases [9]. The work of [10] focuses on designing a heat pump loop for manned spacecraft habitats. The authors also mention the importance of phasing out passive thermal transport (heat pipes) and replacing them with active thermal control systems (heat pumps). With recent technological developments in microgravity testing, the work of [11] and [12] focus on gravity insensitive heat pumps that can be used for Lunar applications.

The consensus is that active thermal management systems such as heat pumps are needed for manned Lunar habitats. Much of the early research focused on designing and performing theoretical analyses. There has been a gap in research from the mid-2000s until now regarding thermal management of deep-space habitats. With the advancements heat pump technology in zero and micro-gravity, it is time to start answering habitat specific research questions. Overall, the field lacks numerical and experimental analysis of deep-space habitat thermal management systems.

1.5 Thesis Objectives and Approach

The goal of this work is to develop and validate a heat pump model that is coupled with the IE model to predict the thermal and humidity control of the CPT. This modeling approach has been done numerous times for terrestrial buildings; however, the deep-space application adds complexity due to the extreme temperatures and disruptions experienced by the habitat. To gain a better understanding of thermal control systems in extraterrestrial habitats, the following research goals have been identified:

- Develop and optimize a heat pump model based on physical dimensions of heat exchangers and data provided by compressor manufacturer
- Conduct a mass balance on the heat exchangers and IE model to predict changes in humidity
- Establish an experimental setup and safety operating procedure for running experiments
- Perform experiments to validate the model with data acquired from varying thermal and moisture loads
- Conduct a parametric study investigating the effects of component size, temperature and pressure

This work is divided into five additional chapters to outline the research goals. Chapter 2 delves into the theory and inspiration for developing the heat pump model. Chapter 3 discusses the experimental setup and data acquisition. Chapter 4 presents results and validation of the model. In Chapter 5, the results of the parametric study will be presented. Finally, Chapter 6 summarizes the work and its key findings as well as suggestions for future work.

2. MODEL METHODOLOGY

2.1 Motivation

Experiments conducted in the laboratory are often the most accurate and are able to show the true performance of a physical system. Despite this, physical experimentation has its limitations. For instance, the number of experiments that can be conducted over a period of time is very limited. The solution to this problem is numerical simulations; they are able to capture the dynamics of the thermal system as well as the entire habitat. The overarching outcome for developing a thermal system model is so that it can be implemented into an entire system model: the modular coupled virtual testbed (MCVT). The MCVT will have the dynamics of the transfer systems to apply interface conditions to the physical subsystems. All physical subsystem models, including the thermal system model, will incorporate experimental observations thus increasing the accuracy of simulating the real systems' behavior. The goal of the MCVT is to answer research questions, in real-time, without having to perform physical experiments. Thermal experiments require substantial time and energy to perform. Conducting a simple heating load experiment can take around 10 hours to complete. Using the CPT as example, the thermal transfer panels must reach steady-state and be in thermal equilibrium with the IE. Once that is achieved the thermal management system can be turned on and data can start being acquired. To this end, all of the time spent, and energy consumed can be mitigated by numerical simulation via the MCVT.

2.1.1 Literature Review

Cyber-physical testing is essentially hardware-in-the-loop (HIL) testing with feedback. The goal is to produce a realistic integrated testbed environment. HIL has been used extensively in the automotive and aerospace industry due to the complexities of the systems. It has many advantages such as low cost, accurate results and reduced risks associated with failure [13]. Figure 3 presents a comparison of different heating system analyses using numerical simulation, hardware only, and HIL.

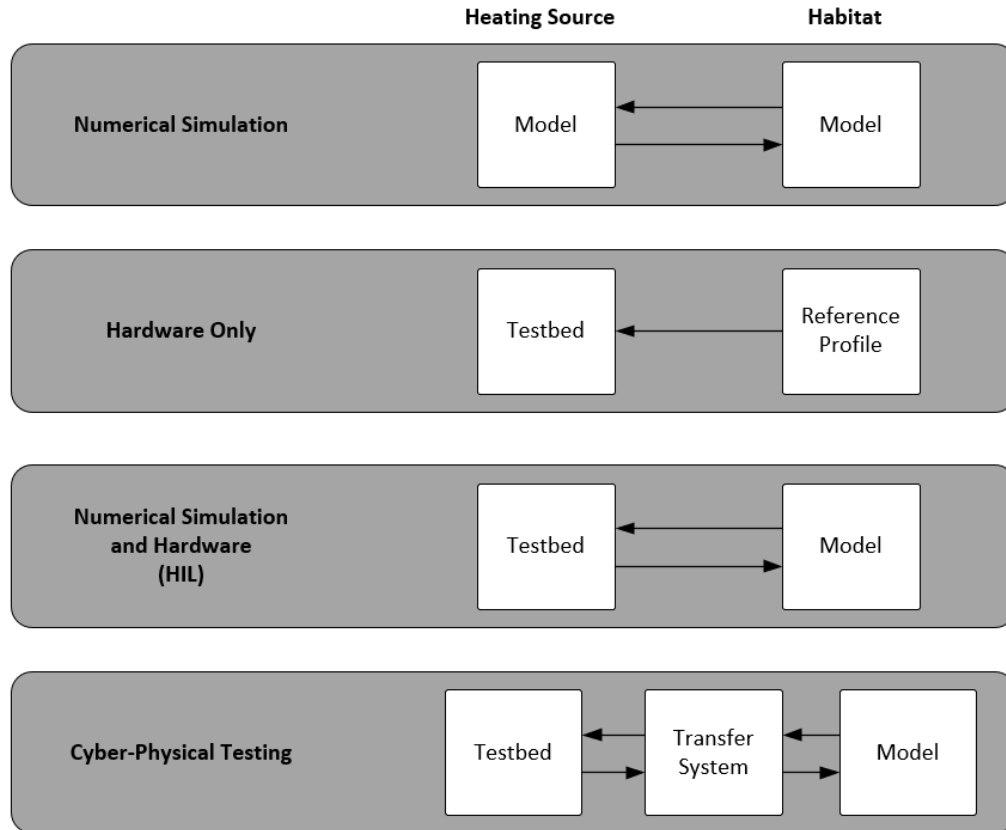


Figure 3: Representation of Heating System Analyses

A plethora of HIL publications are available for automotive, power and radar systems, but there are a limited number of publications that discuss heating, ventilation and air conditioning (HVAC) systems. Among these publications is the work of [14], where HIL simulations were used to test control algorithms for improving the energy consumption of HVAC systems in buildings. In [15], [16], and [17], HIL systems were used to estimate and optimize heat pump systems coupled to thermal storage tanks. These works focused on improving energy efficiency and minimizing on/off cycling of heat pumps.

2.1.2 Heat Pump Modeling Inspiration

The goal of the heat pump model is to accurately predict heat transfer rates and power consumption. RETHi's main interest, with regards to the thermal system, is how it will affect other subsystems. Therefore, an advanced heat pump model that predicts every aspect of the vapor compression cycle (VCC) with high accuracy is unnecessary. For that reason, a semi-empirical

model that is able to map the performance of the heat pump will be implemented. This hybrid modeling approach is simple to implement and does not require in-depth understanding of the system physics [18]. Since the heat pump to be modeled was provided to RETHi from Mitsubishi Electric, the semi-empirical modeling approach is suitable given that sufficient training data exists [19].

2.2 Heat Pump Cycle Model

The semi-empirical quasi-steady state heat pump model is constructed in a functional programming fashion within MATLAB [20]. The model considers the four basic components of the VCC: evaporator, compressor, condenser, and expansion valve. For reference, a four component VCC with state points is shown in Figure 4. The assumptions made during the modeling process include isenthalpic expansion, no pressure drops through the heat exchangers and constant degree of superheat and subcooling. Assuming constant degree of superheat and subcooling implies that the system has a perfect expansion valve and correct refrigerant charge respectively. In order for the model to execute, the user must define the operating conditions of the heat pump by inputting the indoor and outdoor steady state sink temperatures as well as the degree of superheat and subcooling.

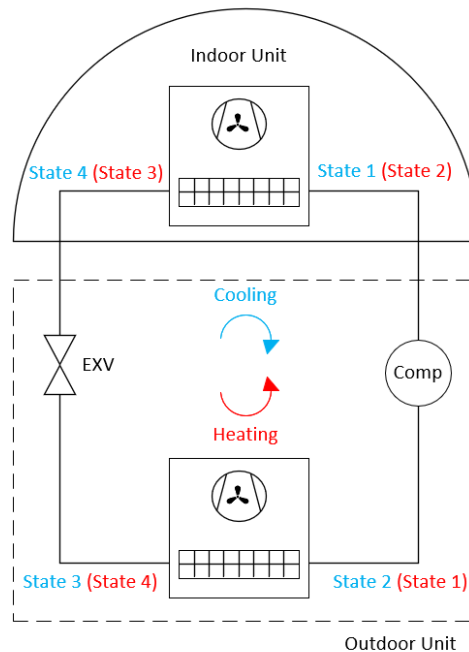


Figure 4: Four Component Vapor Compression Cycle with State Points

The heat pump cycle contains four component sub-models: evaporator, compressor, condenser, and expansion valve. The structure for information flow of the component sub-models can be seen in Figure 5.

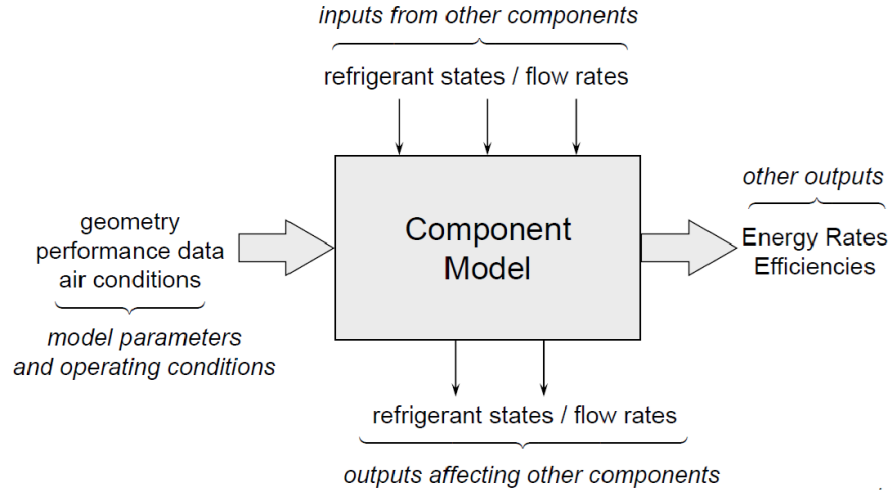


Figure 5: Structure for Information Flow of the Component Sub-Models

Simulating a heat pump with component models results in two residuals: enthalpy at state points two and four. The enthalpy of state point two is an output of both the compressor and condenser sub models. Similarly, the enthalpy of state point four is the output of the evaporator and expansion valve sub models. In order for the model to converge, the residuals must be minimized. A residual vector was defined by Equation 1, $\vec{\Delta}$ is the defined residual vector for cycle convergence, $h_{2,comp}$ is the state point (2) enthalpy output from the compressor model, $h_{2,cond}$ is the state point (2) enthalpy output from the condenser model, $h_{4,ev}$ is the state point (4) enthalpy output from the expansion valve model, and $h_{4,evap}$ is the state point (4) enthalpy output from the evaporator model

$$\vec{\Delta} = \begin{bmatrix} |h_{2,comp} - h_{2,cond}| \\ |h_{4,ev} - h_{4,evap}| \end{bmatrix} \quad (1)$$

The residual vector was minimized via the built-in MATLAB minimization function: `fmincon`. There is not a preconditioner present in the model therefore it requires the user to make an initial guess of the evaporating and condensing temperatures. Thermophysical properties for

R410A are calculated using CoolProp [21]. Executing the model results in outputs: evaporating and condensing temperatures, heat transfer rates of the heat exchangers, work consumed by the compressor, and coefficient of performance.

The flowchart of the heat pump cycle algorithm can be seen in Figure 6. The user provides inputs and makes an initial guess for the evaporating and condensing temperatures. The inputs and initial guess values are sent to the heat pump model. The compressor sub-model executes first in order to output the mass flow rate needed for the heat exchanger sub-models. The order in which the remaining sub-models execute is not critical; however, it was chosen to execute them following the order of the VCC state points: condenser, expansion valve, and evaporator. Execution of the sub models results in the enthalpy residual vector. The minimization function executes; if the residual vector is within the tolerance the model is complete, conversely if the vector is outside the tolerance new guesses are made for evaporating and condensing temperatures and the process repeats until tolerance is met. Once the model is complete the desired parameters are output.

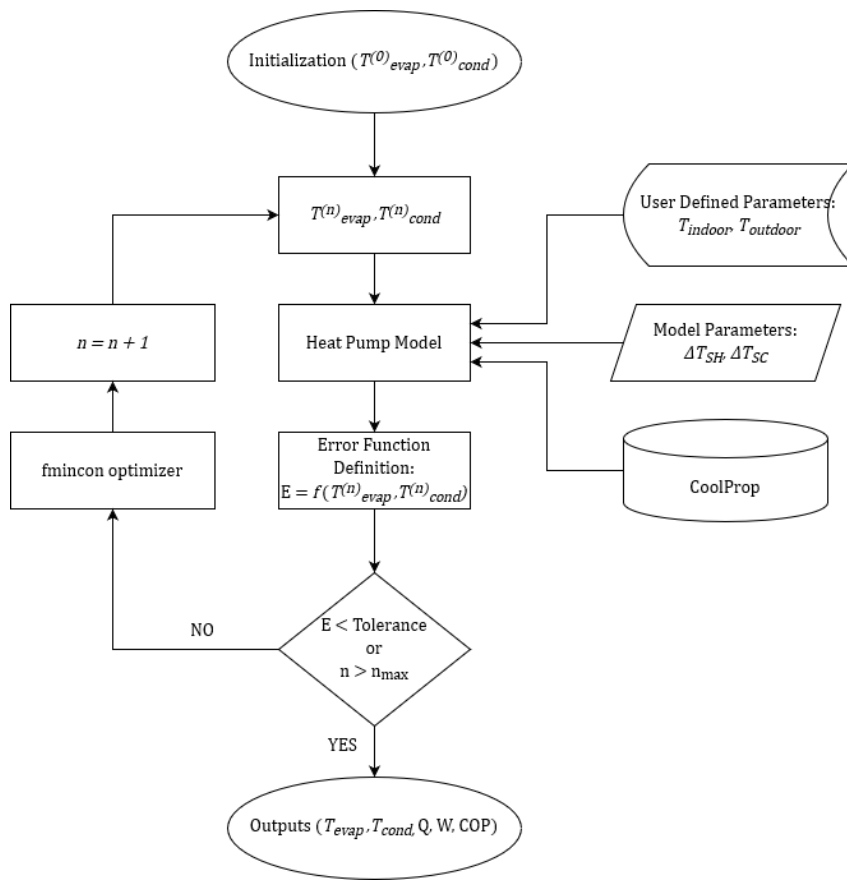


Figure 6: Heat Pump Cycle Solver Algorithm

2.2.1 Evaporator Model

The modified evaporator model from [22] was constructed using the lumped method which assumes the evaporator is entirely two-phase refrigerant. The entire heat exchanger is simulated using the ϵ -NTU method [23] and assumes that the constant pressure is equal to saturation pressure. In order to accurately predict the heat transfer on the air-side of the heat exchanger, the partially-wet/partially-dry method was used from [24]. The evaporator is separated into two separate lumped analyses—fully wet and fully dry—as shown in Figure 7. The separation position between wet and dry area is iteratively determined by analyzing the point where the evaporator surface temperature is equal to the dewpoint temperature of the moist air.

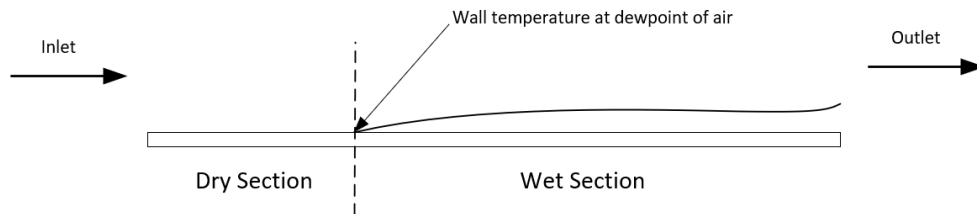


Figure 7: Schematic of Evaporator Model Displaying Partially Wet/Partially Dry Analysis

The correlations used to solve the air-side and refrigerant-side heat transfer coefficients are [25] and [26], respectively. The air-side Nusselt number is a function of Reynolds number, Prandtl number and the ratio of heat exchanger surface area to unfinned surface area. The Nusselt number can then be used to solve for the heat transfer coefficient. The refrigerant-side heat transfer correlation is a function of convection number and boiling number. An average refrigerant quality of 0.5 was assumed for the convection number. The measured geometrical parameters used for the correlations are presented in Table 1.

Table 1: Geometrical parameters in evaporator model

Number of tubes	40
Length of tubes [mm]	737
Outer diameter of tubes [mm]	6.35
Inner diameter of tubes [mm]	4.83
Longitudinal distance of tubes [mm]	19.1
Transverse distance of tubes [mm]	12.7
Fins per inch	20
Fin thickness [mm]	0.203
Conductivity of fins [W/m-K]	237

2.2.2 Compressor Model

The continuous modulating compressor was modeled using a modified form of the AHRI 540 standard polynomial equation [27] represented by Equations (2) and (3) where \dot{W}_{comp} is the power consumed by the compressor, \dot{m}_{suc} is the mass flowrate entering the compressor, c_i are the linear regression coefficients, T_{evap} is the evaporating temperature, T_{cond} is the condensing temperature, and Hz is the rotational speed of the compressor.

$$\begin{aligned} \dot{W}_{comp} = & c_1 + c_2 T_{evap} + c_3 T_{evap}^2 + c_4 T_{evap}^3 + c_5 T_{cond} + c_6 T_{cond}^2 + c_7 T_{cond}^3 + c_8 Hz \\ & + c_9 Hz^2 + c_{10} Hz^3 + c_{11} T_{evap} T_{cond} + c_{12} T_{evap} T_{cond}^2 + c_{13} T_{evap} Hz \\ & + c_{14} T_{evap} Hz^2 + c_{15} T_{evap}^2 T_{cond} + c_{16} T_{evap}^2 Hz + c_{17} T_{cond} Hz \\ & + c_{18} T_{cond} Hz^2 + c_{19} T_{cond}^2 Hz \end{aligned} \quad (2)$$

$$\begin{aligned} \dot{m}_{suc} = & c_1 + c_2 T_{evap} + c_3 T_{evap}^2 + c_4 T_{evap}^3 + c_5 T_{cond} + c_6 T_{cond}^2 + c_7 T_{cond}^3 + c_8 Hz \\ & + c_9 Hz^2 + c_{10} Hz^3 + c_{11} T_{evap} T_{cond} + c_{12} T_{evap} T_{cond}^2 + c_{13} T_{evap} Hz \\ & + c_{14} T_{evap} Hz^2 + c_{15} T_{evap}^2 T_{cond} + c_{16} T_{evap}^2 Hz + c_{17} T_{cond} Hz \\ & + c_{18} T_{cond} Hz^2 + c_{19} T_{cond}^2 Hz \end{aligned} \quad (3)$$

The third-order polynomial equation is used to present the published ratings from Mitsubishi Electric. It uses 19 coefficients due to the power and mass flow rates being functions of evaporating temperature, condensing temperature and compressor rotational speed. The coefficients of the mass flow rate and the power consumption correlations are estimated by the method of least squares. The estimated compressor model coefficients are listed in Table 2 along with the R^2 values. Corrections for other superheat temperatures other than specified in the compressor data have been made using [28].

Table 2: Compressor Mapping coefficients

	c_1	c_2	c_3	c_4	c_5	c_6	c_7	c_8	c_9	c_{10}
\dot{W}_{comp} (W)	3322.157	-47.239	0.681	4.321×10^{-6}	184.532	-3.585	0.024	30.874	-0.361	1.573×10^{-3}
\dot{m}_{suc} (kg/h)	64.684	0.107	-0.022	2.688×10^{-4}	-3.853	0.077	-5.089×10^{-4}	1.597	2.501×10^{-3}	1.210×10^{-5}
	c_{11}	c_{12}	c_{13}	c_{14}	c_{15}	c_{16}	c_{17}	c_{18}	c_{19}	R^2
\dot{W}_{comp} (W)	1.077	-2.316×10^{-3}	0.068	5.498×10^{-4}	-0.012	-8.570×10^{-3}	-0.129	3.441×10^{-3}	2.869×10^{-3}	0.99
\dot{m}_{suc} (kg/h)	0.011	-1.954×10^{-4}	0.045	1.686×10^{-4}	2.506×10^{-4}	9.597×10^{-4}	-2.966×10^{-3}	-1.850×10^{-5}	-2.558×10^{-5}	1

2.2.3 Condenser Model

The condenser model was also modified from [22] and uses the lumped method. The entire heat exchanger is simulated using the ϵ -NTU method [23] assuming the constant pressure is equal to inlet pressure. The air-side correlation [25] used in the evaporator model was also used for the condenser model. The refrigerant-side correlation used is [29]. It is a function of liquid heat transfer coefficient, quality and Prandtl number. An average refrigerant quality of 0.5 was assumed. The measured geometrical parameters used for the correlations are presented in Table 3.

Table 3: Geometrical parameters in condenser model

Number of tubes	80
Length of tubes [mm]	889
Outer diameter of tubes [mm]	6.35
Inner diameter of tubes [mm]	4.83
Longitudinal distance of tubes [mm]	22.2
Transverse distance of tubes [mm]	21.0
Fins per inch	20
Fin thickness [mm]	0.203
Conductivity of fins [W/m-K]	237

2.2.4 Expansion Valve Model

The expansion valve is assumed to be a constant enthalpy throttling process. This assumption is valid due to there being no work received or produced and the absence of heat being exchanged with the surroundings [30]. Similarly, during steady state and steady flow operation the assumption holds true. Lastly, kinetic, and potential energy changes at the inlet and outlet of the valve are neglected. All of these concepts can be applied to the electronic expansion valve.

2.2.5 Fan Model

Both the evaporator fan and condenser fan run at a fixed speed. The airflow and power consumption were not measured but taken from the manufacturer data sheet. The evaporator flow rate and power consumption are $0.816 \text{ m}^3/\text{s}$ and 33 W respectively. The condenser flow rate and power consumption are $0.217 \text{ m}^3/\text{s}$ and 252 W respectively. Both fans were modeled using these values for steady-state operation.

3. CYBER-PHYSICAL TESTBED THERMAL MANAGEMENT SYSTEM

3.1 Experimental Setup

The heat pump cycle model is validated by conducting experiments on the cyber-physical testbed set up. The CPT currently consists of a prototype of an extra-terrestrial habitat at one-fifth scale. The habitat's structure is a geodesic dome. Inside the dome is an inflatable bladder that replicates the IE of the habitat. The prototype of the habitat is displayed in Figure 8. Triangular thermal transfer panels (Figure 9) are to be placed within the dome's structure to replicate external regolith dynamic response, thus imposing a load on the heat pump.



Figure 8: Habitat Prototype Consisting of Geodesic Dome and Inflatable Bladder



Figure 9: Triangular Thermal Transfer Panel

The indoor unit is positioned inside the bladder. The refrigeration lines are fed through access ports to the outdoor unit which resides outside of the bladder. In heating mode, heat is sourced from the large open area of the laboratory. The heat is then transferred to the evaporating refrigerant flowing through the outdoor heat exchanger. The refrigerant is compressed to higher pressure and rejected to the interior of the bladder via condensing refrigerant flowing through the indoor heat exchanger.

3.1.1 Data Acquisition Setup

In order to characterize the heat pump and validate the model, sensors and thermocouples are to be instrumented. Temperature and pressure measurements need to be taken at the inlet and outlets of the heat exchangers to define the state of the working fluid thus providing an enthalpy. The measurements correspond to the four state points defined in the model. A mass flow meter is needed to measure the mass flow of the refrigerant. Mass flow rate data will be used to calculate the heat transfer rates of the heat exchanger. A detailed heat pump refrigerant-side sensor set up is presented in Figure 10. A power transducer was installed to measure the total power consumed by

the heat pump. The entire experimental setup schematic is shown in Figure 11. The list of sensors used, and their tolerances can be found in Table 4.

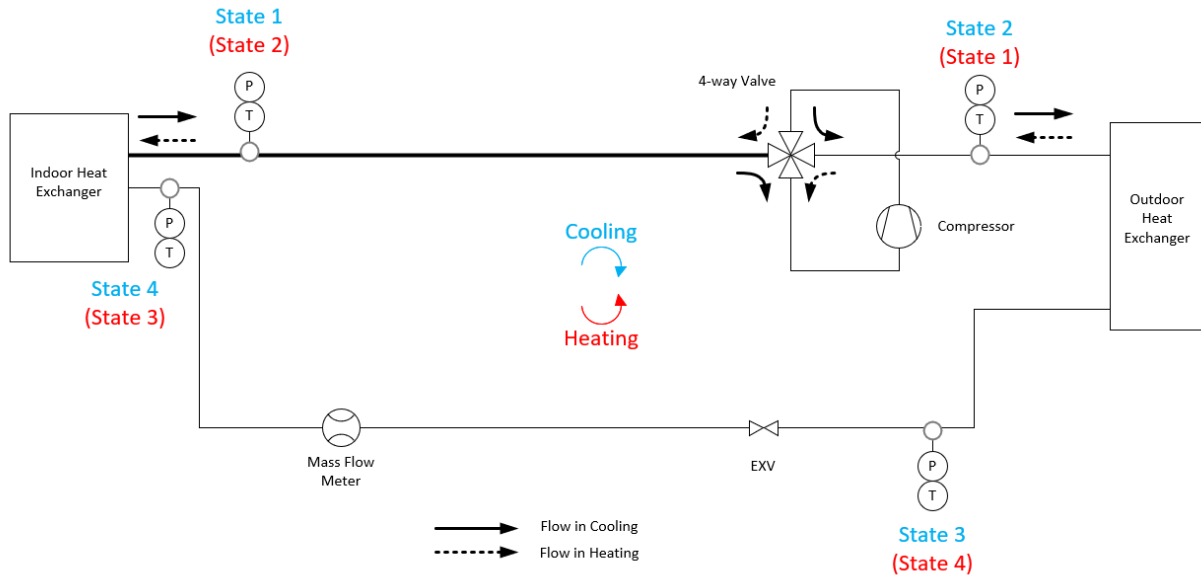


Figure 10: Heat Pump Sensor Schematic

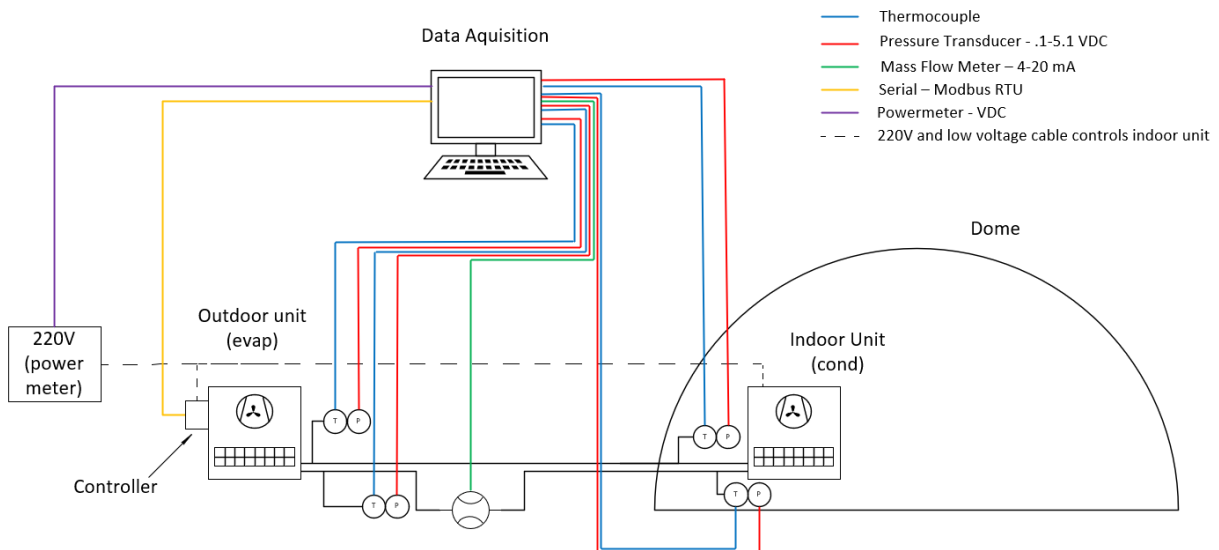


Figure 11: Experimental Setup with Wiring Schematic

Table 4: List of Sensors with Specifications and Tolerances

Sensor	Specifications	Accuracy
Omega T-Type Thermocouple Probe	-200 to 350°C	±1.0K
Setra Model 207 Pressure Transducer	0 to 500 psig	±0.65 psig
Omega Relative Humidity Sensor	0-100% RH	±1% RH
Emerson Micro Motion Elite Coriolis Mass Flow Meter	0 to 110 kg/hr	±0.2% Rdg.
Ohio Semitronics Model GW5 Watt Transducer	0 to 20 kW	±0.2% Rdg.

Data acquisition is accomplished through a m+p analog input module. Its hardware accepts positive and negative voltages. The voltages are read, and Simulink Real-Time code is developed to apply a gain and offset if needed to accurately produce the correct output. Reading thermocouple data requires a m+p international DAQ. Figures 12 and 13 display thermocouples and sensors connected to their respective I/O modules. All sensors were calibrated in the laboratory before installing them onto the refrigeration piping.

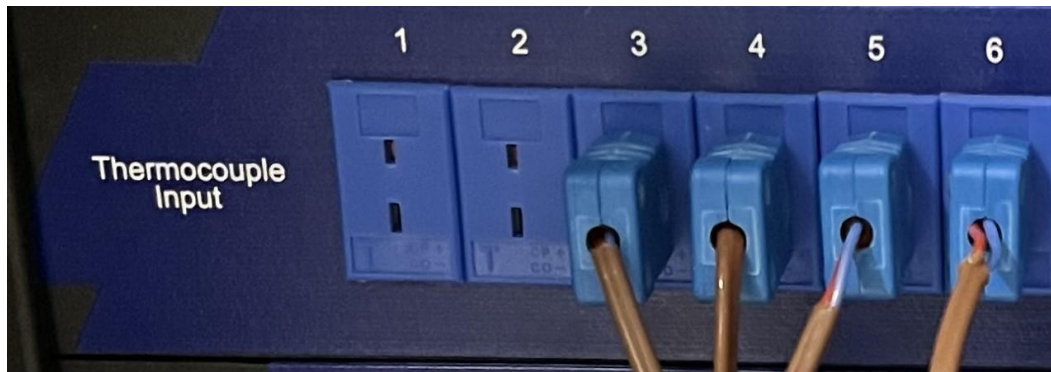


Figure 12: Thermocouple Inputs to I/O Module



Figure 13: Sensor Inputs to Voltage I/O Module

3.1.2 Modbus Control Setup

A requirement of the CPT is for the heat pump to be controlled through Simulink Real-Time. Communication between the Speedgoat Performance Real-Time Target Machine and the heat pump is possible through Modbus protocol. Mitsubishi offers a controller that is powered and interfaced to the indoor unit's electronic control printed circuit board. The controller allows for remote control and monitoring of the heat pump. The controller uses Modbus RTU (serial) however, Speedgoat's communication I/O modules support Modbus TCP (ethernet). For this reason, an external networking gateway is needed. The gateway establishes a server on the same network as the Speedgoat Real-Time Target Machine and allows connection from the Modbus RTU slave to the Modbus TCP client. The setup of the Modbus slave gateway can be seen in Figure 14 below. It is worth noting that the slave, gateway and Speedgoat Real-Time Target Machine all reside on the same network, with different IP addresses, handled by an ethernet switch.

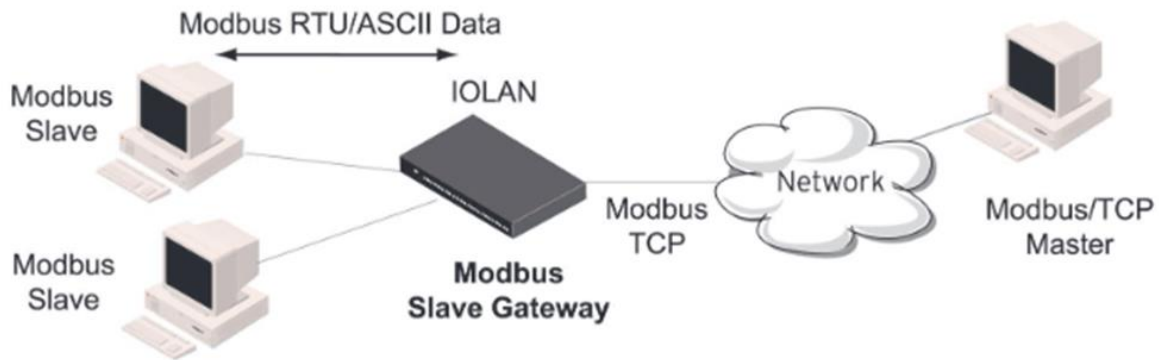


Figure 14: Modbus Slave Gateway Connection Schematic [31]

Modbus is an open communication protocol that follows a master-slave architecture. Masters are responsible for sending commands to slave devices and reading data. Slaves simply do nothing until a command is sent from the master; the slave will act upon that command and send a reply to the master. Modbus slaves store data in registers. The scope of the heat pump experiments only requires the use of holding registers which are analogue outputs. Holding registers are read and write accessible which hold information in a 16-bit unsigned integer value.

3.2 Heat Pump Control Simulink Model

Establishing a connection between the Speedgoat Real-Time Target Machine, the heat pump and reading/writing holding registers requires development of Simulink code. First, a Modbus TCP client setup block is needed. It has station ID and host IP address as parameters. The station ID is an internal naming convention for the code and is set to 0. The host IP address is the real-time target machine's IP address. Next, a Modbus TCP client connection block is needed. The important parameters are station ID, sample time and remote IP address. The station ID is set to 0 and the remote IP address is the slave IP address which was configured via the gateway. The client connection block has one Boolean output that displays whether a connection is made or not. The setup and connection Simulink code can be seen in Figure 15.

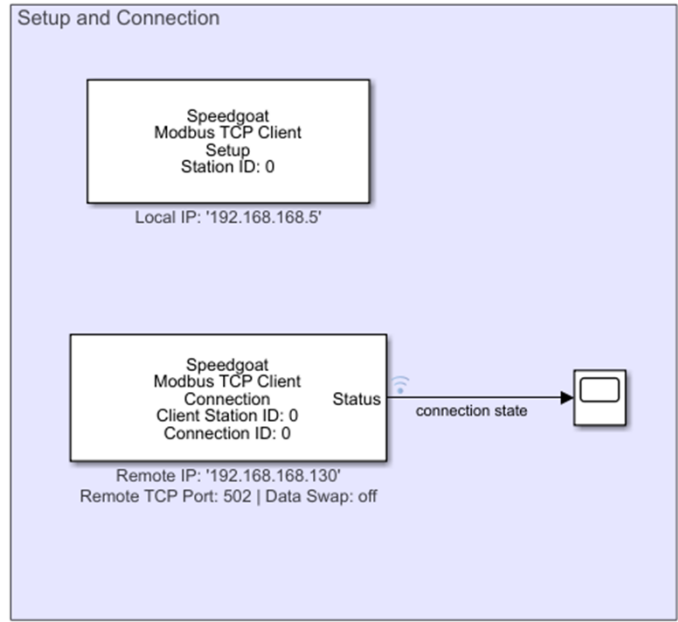


Figure 15: Setup and Connection Simulink Code

Finally, a Modbus client transceiver block is needed in order to read/write the holding registers. An example of writing to a holding register via Simulink code can be observed in Figure 16. A byte packing block is used to pack the signal that the Speedgoat Real-Time Target Machine sends to the controller. Since the input is in big endian format, a byte reversal block is needed to swap the bytes.

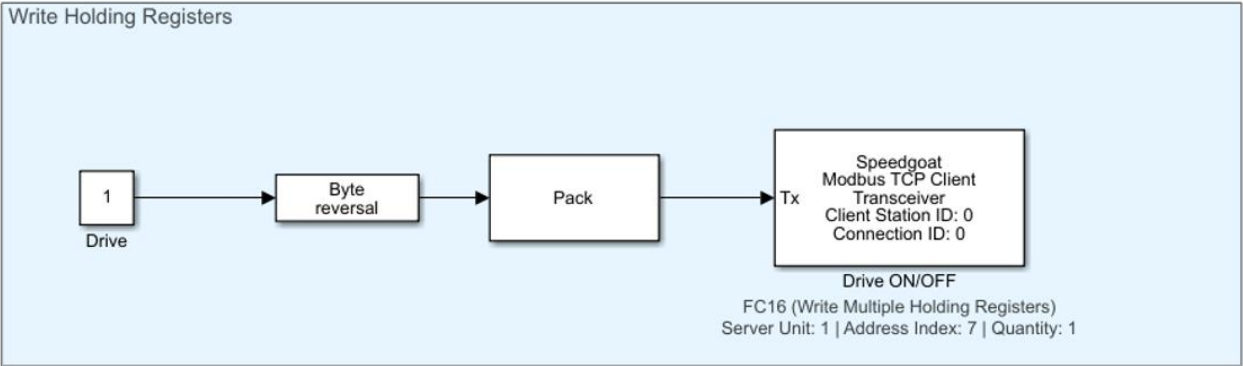


Figure 16: Writing a Holding Register Simulink Code

A control panel was developed to turn the heat pump on and off, select operation mode (heating or cooling), input an operating setpoint temperature, and select a fan speed. The control panel allows the user to control the heat pump easily without having knowledge of the Simulink code. The graphical user interface is shown in Figure 17.

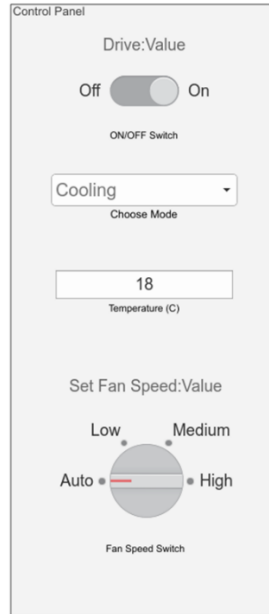


Figure 17: Heat Pump Control Panel

3.3 Heat Pump Data Acquisition Simulink Model

Acquiring the necessary data to validate the heat pump model requires creating a hardware/software interface. The tool used to read the voltage and thermocouple signals from the I/O modules is m+p dynamic signal analyzer. The analyzer is capable of gathering data and displaying results at user defined frequencies. The thermocouples and sensors are enabled with their respective channels within the software. An application programming interface (API) was developed by other members of the RETHi team in order to store and visualize the data in real time. The API, developed by [32], communicates with the m+p dynamic signal analyzer to send raw data to Simulink. Within Simulink, the raw voltage data is converted into physical units and displayed in real time. After an experiment is performed, the data is then stored in a .mat file for further, detailed analysis. Screenshots of the Simulink data acquisition code and m+p dynamic signal analyzer are displayed in Figures 18 and 19.

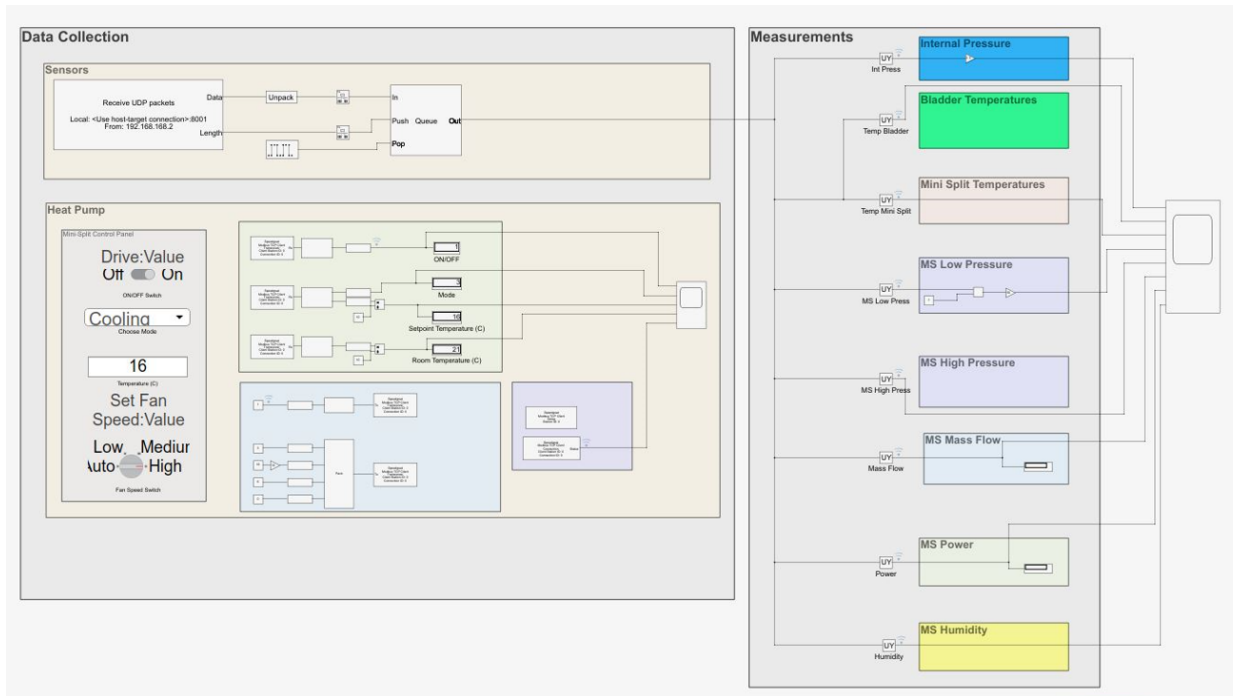


Figure 18: Screenshot of Simulink Control Panel with Data Acquisition

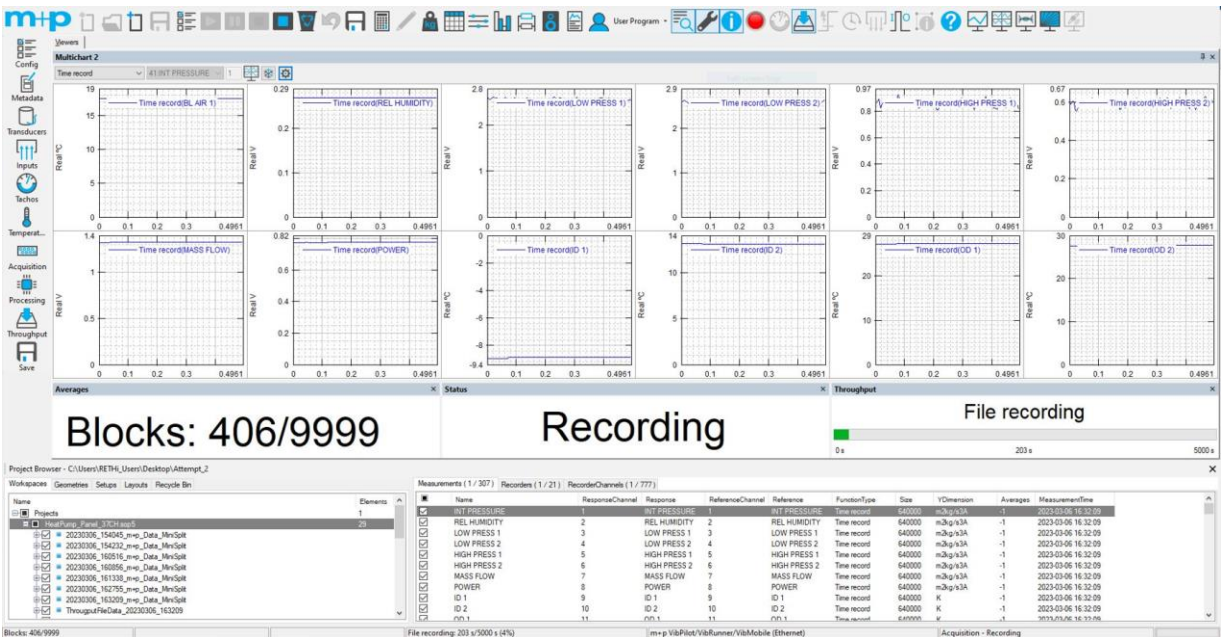


Figure 19: Screenshot of m+p Dynamic Signal Analyzer

3.4 Heat Pump Experimental Procedure

The R410A charged heat pump serves as the heating and air conditioning system for the CPT. The system's primary goal is to transfer heat into or out of the dome in order to meet a setpoint temperature. The heat pump will handle a variety of thermal loads which will be imposed by the chiller and transferred to the habitat via thermal transfer panels. Varying thermal loads (latent and sensible) and anomalies need to be understood in order to create a more accurate and reliable environmental control and life support system (ECLSS) model. This research will characterize the heat pump, determine its limitations, and understand its behavior when an anomaly occurs.

Little information is known about implementing an air-to-air heat pump in an environment with extreme boundary conditions. Similarly, the behavior of the system when a failure occurs is unknown. To gain a further understanding of the system and be able to develop a model, experimentation is needed. The goal of heat pump experimentation is to (1) map the performance with varying loads (sensible and latent) (2) measure power consumption and heat transfer rates (3) test failure modes and how they affect the IE. After conducting these experiments, the model will be validated based on how the system will behave given different conditions. In order to perform experiments safely and repeatably, an operating procedure was created and is located in Appendix A.

3.4.1 Preliminary Experimentation

A set of preliminary experiments has been defined and are to be performed with the absence of the substantial load provided by the thermal transfer panels. These preliminary experiments are needed to determine the amount of time to reach a setpoint temperature from cold soak initial condition, characterize the cyclic operation of the heat pump and assure all sensors are working properly and recording accurate data. The cyclic operation of the heat pump occurs due to the absence of a load. During these experiments, the heat pump will overshoot the set point temperature and shut off. Due to the small thermal inertia of the CPT habitat, the heat will exit the system resulting in the interior temperature dipping below the setpoint temperature. The research question to be answered is how quickly the CPT habitat loses heat in its current state. If heat is lost too quickly (less than three minutes), the heat pump will fail to turn on due to its compressor

protection logic programmed into the control board. The time delay function operates to protect the compressor from overload. The three-minute delay is also important in a disturbance scenario. For example, if the heat pump shuts off during normal operation at a similar time at which an anomaly occurs in the habitat that requires thermal management, the heat pump will not be able to respond until the protection delay time has elapsed. The test plan is outlined in Table 5.

Table 5: Preliminary Experimental Test Plan

Initial Dome Temperature	Set Point Temperature (°C)	Mode	Fan Speed
Lab Ambient	16	Cooling	High
Lab Ambient	27	Heating	High

3.4.2 Model Validation Experiments

Due to there not being a load imposed on the IE and cyclic operation of the preliminary experiments, model validation will be nearly impossible due to the heat pump never entirely reaching steady state. In order to impose cooling and latent loads on the CPT IE, electric heaters and a warm mist humidifier are used. The heaters are capable of outputting 2500 W which exceeds the minimum capacity (1800 W) of the heat pump. Similarly, the name plate power rating of the humidifier is 400 W. Due to the dry conditions of the lab, the humidifier allows moist air to be produced until the desired relative humidity is reached. The heat pump will be turned on in cooling mode once the IE reaches a steady state condition. Since the load applied is only 700 W above the minimum capacity, experiments will be performed with the fan speed set on low to allow for a steady state condition to be reached. Imposing a heating load on the CPT IE requires at least a single thermal transfer panel that is installed on the habitat and connected to the chiller. The chiller will be started and allowed to reach the desired setpoint temperature of the thermal transfer panel. When the panel reaches its setpoint, the heat pump will be turned on and data will be acquired. The purpose of this experiment is to determine the amount of time to reach an IE setpoint temperature from hot/cold soak initial condition and acquire performance data for heat pump under an imposed load to validate the model. A schematic of the CPT, chiller, heater and humidifier are displayed in Figure 20.

The test plan for the cooling model validation experiments is outlined in Table 6. The first experiment simulates an unmanned, no disturbance scenario. There is no moisture addition into the habitat and the cooling load is expected to be purely sensible. The second experiment simulates a manned, no disturbance scenario. There is moisture addition due to the respiration and perspiration of humans. The test plan for the heating model validation experiments is shown in Table 7. Both experiments simulate removal of the exterior habitat insulation due to a disturbance. Two different panel temperatures are tested to vary the loads imposed on the IE. Each test condition is to be performed at least three times to assure repeatable and accurate data is acquired.

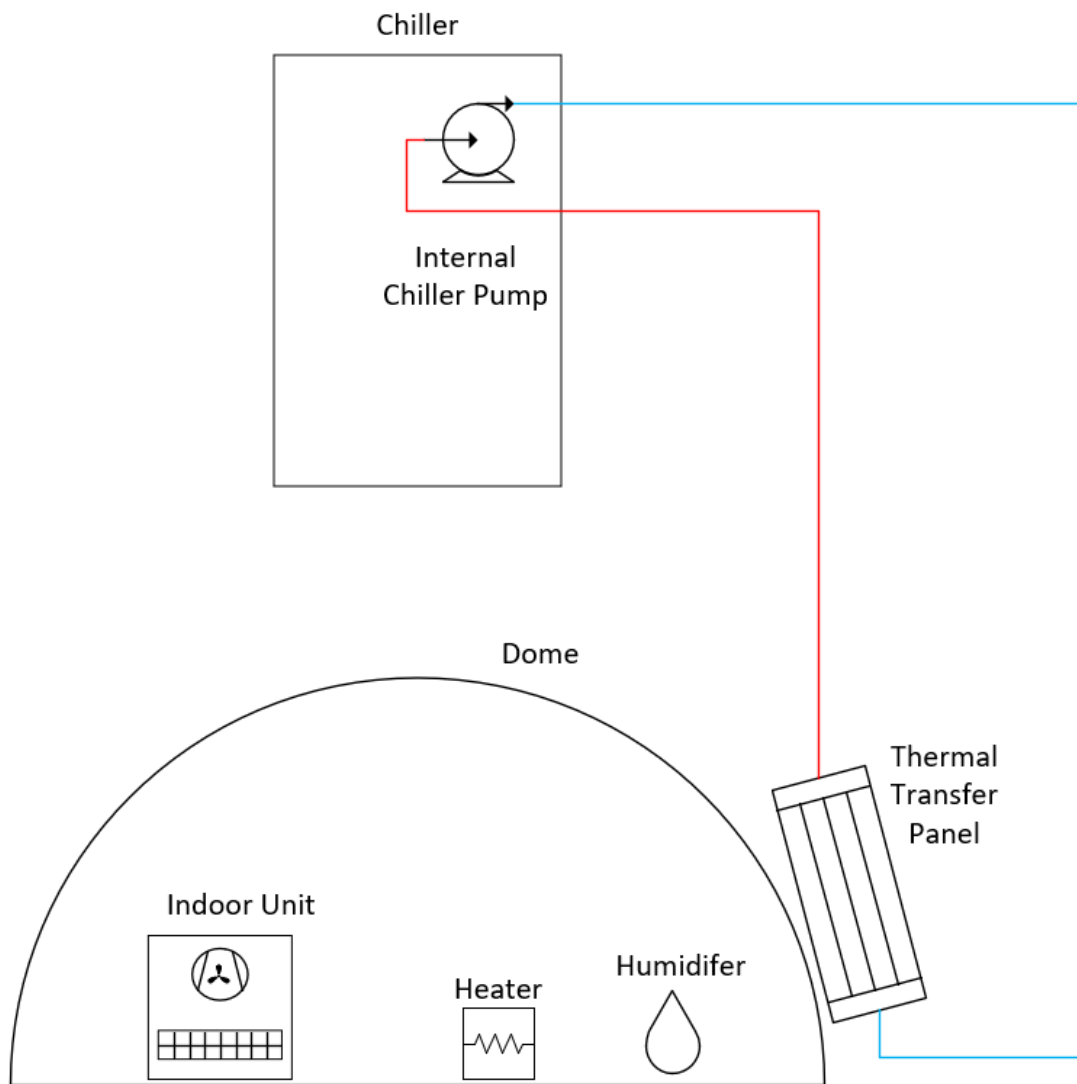


Figure 20: Schematic of Testbed During Model Validation Experimentation

Table 6: Cooling Model Validation Experimental Test Plan

Sensible Load Applied (W)	RH%	Set Point Temperature (°C)	Fan Speed
2500	25%	20	Low
2500	70%	20	Low

Table 7: Heating Model Validation Experimental Test Plan

Single Panel Temperature (°C)	Set Point Temperature (°C)	Fan Speed
-40	27	Low
-60	27	Low

4. RESULTS AND MODEL VALIDATION

4.1 Motivation

This section provides the experimental tests outlined in Chapter 3. The results of two data sets are presented under the no-load test condition. The unit was operated for one hour in order to allow for at least six on/off cycles to occur. Despite this data being unfit for steady state analysis and model validation, it provides insight on the transient dynamics of the system. A total of four data points are presented at steady-state that are used for validating the model. Each of the four data points were repeated three times to assure there were no outliers. The results for all experiments are analyzed and compared in the following section.

4.2 Results

4.2.1 No-Load Experimental Results

The results of the heat pump operating in cooling mode with a setpoint of 16°C as outlined in Table 5 of Chapter 3 are displayed first. The pressures and temperatures of the VCC state points from Figure 10 as well as the bladder air temperature are shown in Figures 21 and 22, respectively.

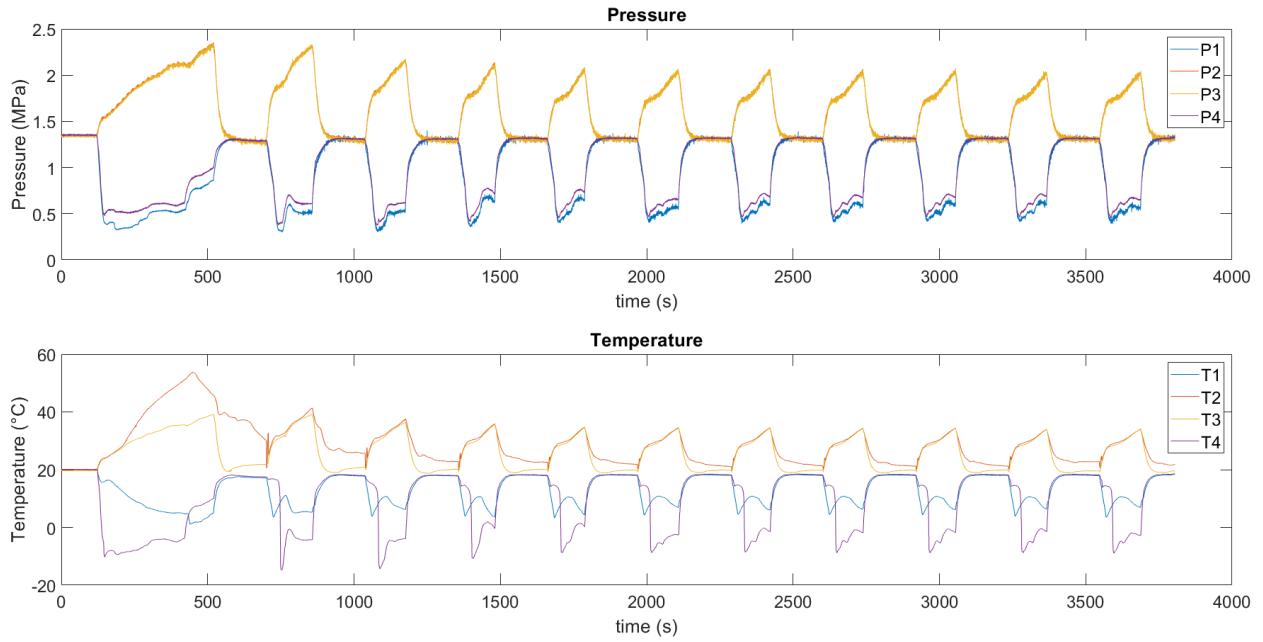


Figure 21: No-Load Cooling Pressure and Temperature vs Time at Cycle State Points

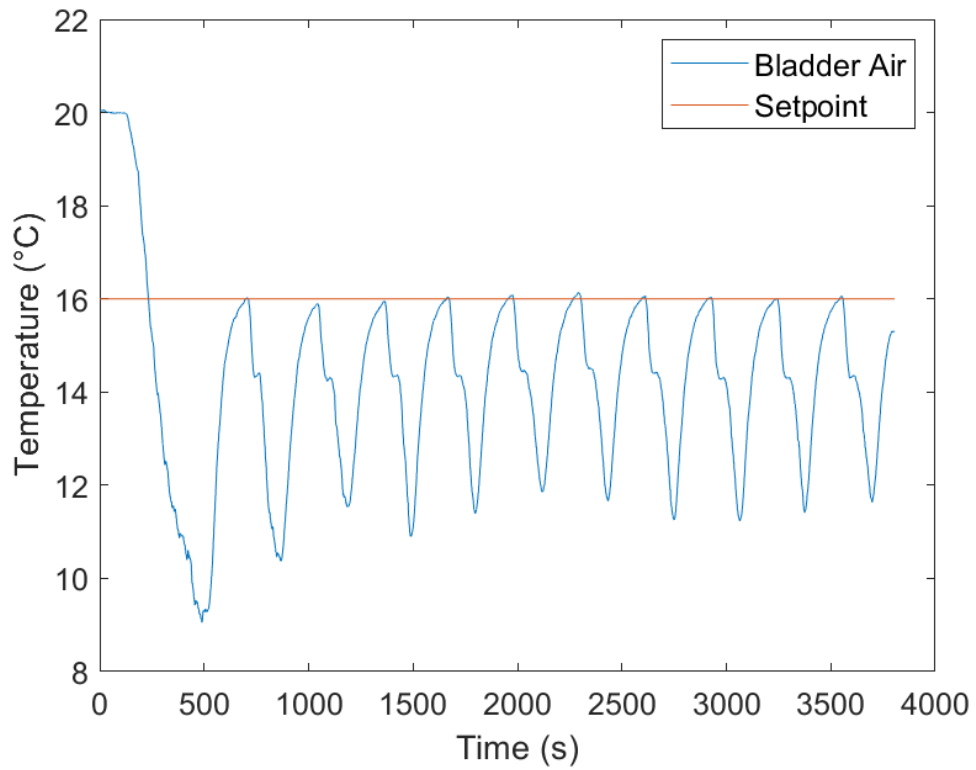


Figure 22: Bladder Air Temperature vs Time in Cooling Mode

The experiments were started at lab temperature (20°C) initial condition meaning the startup of the heat pump experienced the largest amount of heat rejection. The unit was unable to reach a steady state condition before the unit reached its setpoint during the first on cycle. Despite having 7K of superheat, visual observation of the sight glass located at the outlet of the condenser showed two-phase refrigerant flow. Comparing the system performance to the model is impossible due to the inability to predict two-phase refrigerant quality. As shown in Figure 22, the unit's controller overshoots the setpoint by roughly 4K. Despite having no internal heat gains such as humans, lights, or other electronics the habitat experiences external heat gains from the lab. Although not analyzed in detail, the external heat gains can be attributed to infiltration from leaks as well as convection and radiation at the boundary of the habitat. Even though the heat pump has a continuously variable speed compressor, large temperature swings around the setpoint temperature are observed. Lastly, the three-minute delay logic for compressor protection does not play a significant role in this scenario due to the fact that the temperature does not increase above the setpoint. The heat pump is able to consistently keep the bladder air temperature below the setpoint and respond when the external heat gains increase the temperature to a point where the unit calls for cooling.

The results of the heat pump operating in heating mode with a setpoint of 27°C as outlined in Table 5 of Chapter 3 are displayed next. The pressures and temperatures of the VCC state points from Figure 10 as well as the bladder air temperature are shown in Figures 23 and 24, respectively.

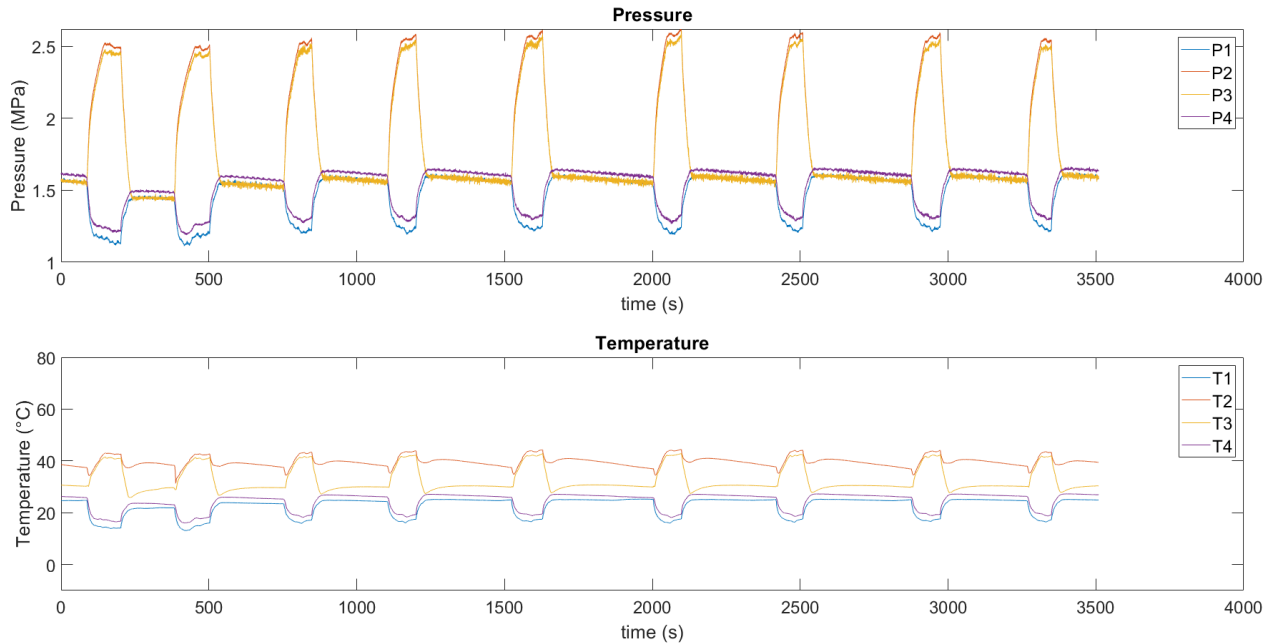


Figure 23: No-Load Heating Pressure and Temperature vs Time at Cycle State Points

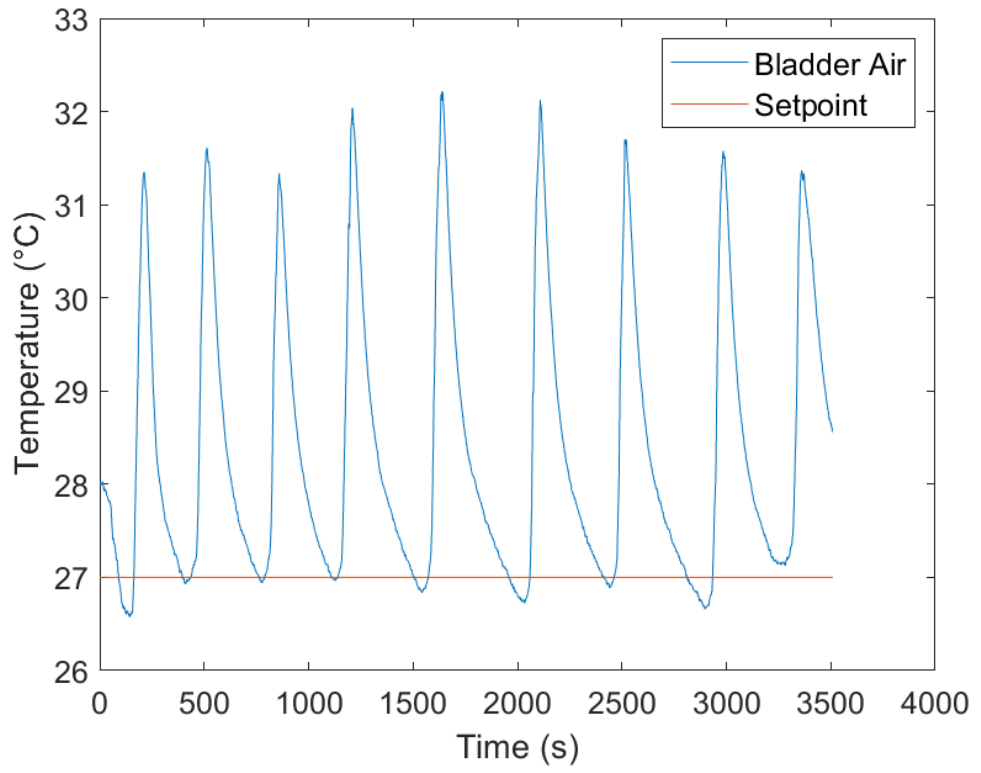


Figure 24: Bladder Air Temperature vs Time in Heating Mode

The experiments were started around the setpoint temperature (28°C). When the heat pump is on, steady state is not reached. In heating mode, there is no superheat at the outlet of the evaporator. This is shown in Figure 23 since there is no temperature difference between state point one and four, meaning the refrigerant is saturated at both the inlet and outlet of the evaporator. Similarly, two-phase flow was observed in the sight glass at the outlet of the evaporator. The lack of superheat can be explained by the heat pump being overcharged in heating mode. Due to the size differences between the indoor and outdoor heat exchangers, a system that has appropriate amount of charge in cooling mode will lead to overcharge in heating mode. The system's accumulator is not large enough to handle the extra liquid refrigerant. Due to space constraints of the testbed, the line set is 4.5 meters. It is recommended by the manufacturer that the line set be no less than 7.6 meters so that the heat pump operates well with factory recommended charge in both heating and cooling mode. Again, large temperature swings of around 5K are observed in the habitat air temperature as seen in Figure 24. External heat losses explain the temperature decrease when the heat pump is off. Lastly, the three-minute delay logic for compressor protection does not play a significant role in this scenario due to the fact that the temperature does not decrease below the setpoint.

4.2.2 Cooling Load Results

During the first test as outlined in Table 6 of Chapter 3, a 2500 W sensible heating load was imposed inside the dome. The relative humidity was initially 25% at 22°C ($\omega = 0.00409$ kg/kg) with no extra latent loads. The target superheat and subcooling was 10K to assure single phase in order to accurately predict the specific enthalpies with temperature and pressure. The pressures and temperatures of the VCC state points from Figure 10, Pressure-specific enthalpy (P-h) diagram at steady state, and bladder air temperature are shown in Figures 25, 26, and 27, respectively.

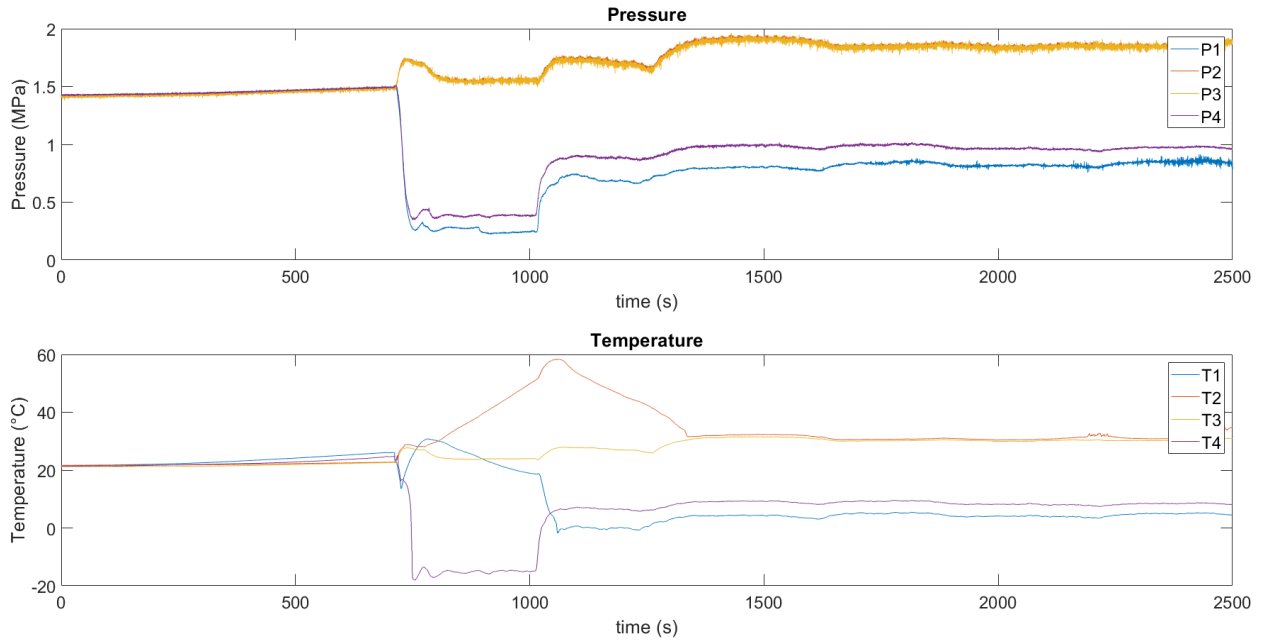


Figure 25: Sensible Cooling Load Test Pressure and Temperature vs Time at Cycle State Points

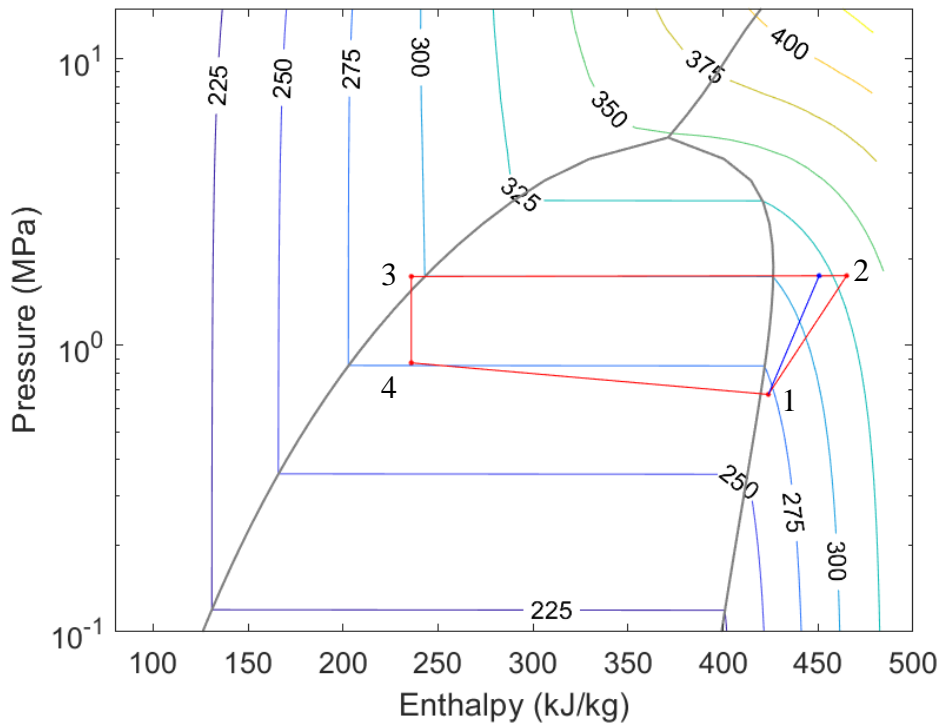


Figure 26: P-h Diagram of Sensible Cooling Load Test at Steady State

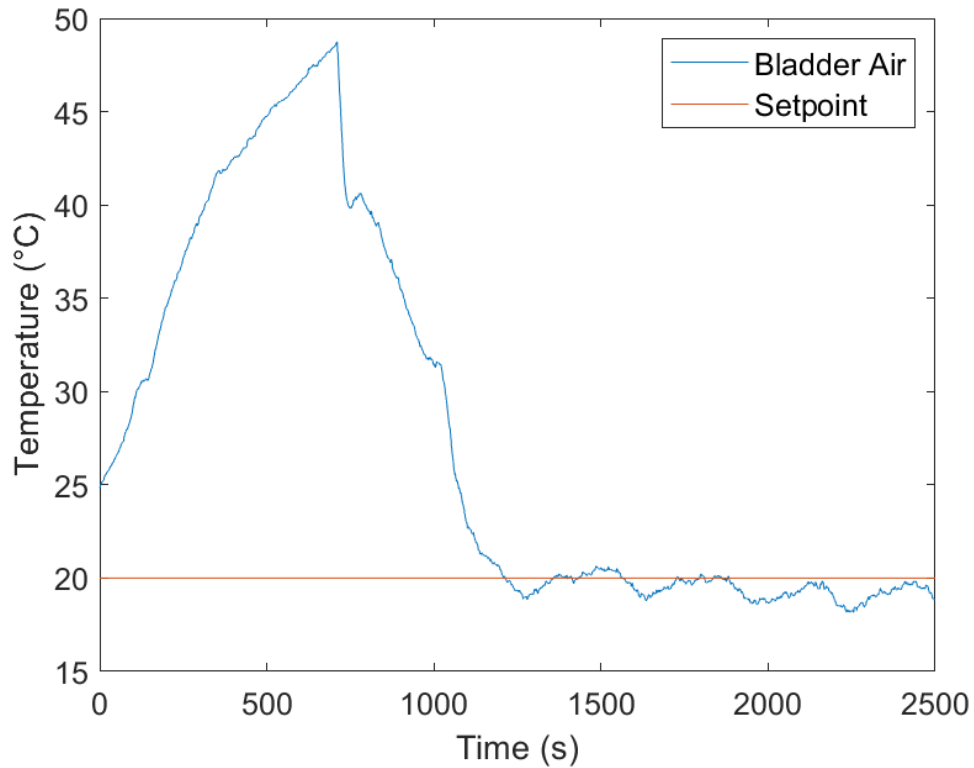


Figure 27: Bladder Air Temperature vs Time During Sensible Cooling Load Test

The sensible load was applied to the habitat at $t = 0$ seconds. The habitat was first allowed to heat up so that the heat pump would reach a steady state operating condition. Due to the high temperature inside the habitat, the heat pump would operate at its rated frequency for long enough in order to not only meet the setpoint but also reach a steady state condition. As shown in Figure 25, the heat pump is turned on at $t = 715$ seconds. The compressor ramps up and hits a peak at $t = 1057$ seconds, and this is the instant at which the cycle operates at “steady state”. A true steady-state operating condition would be shown by a plateau; however, after this peak the compressor starts to slug. During the time period $t = 1057$ to 1340 seconds, the compressor slowly floods as shown by the decrease in discharge temperature. Both flooding and slugging of the compressor can be explained by three factors: (1) low load on evaporator, (2) unoptimized control of electronic expansion valve (EXV), and (3) undersized accumulator. The low load on the evaporator is very possible considering the heat pump operating near the minimum capacity recommended by the manufacturer. The EXV is controlled by logic engineered by the manufacturer. The controller is meant for a residential setting and not a small volume deep space habitat prototype. Unfortunately,

it cannot be reprogrammed in its current state. Because of the low load and uncontrollable EXV, the system's accumulator fills with liquid refrigerant and the suction of the compressor is eventually flooded.

Plotting pressure and enthalpy the instant before the compressor starts to flood results in the P-h diagram shown in Figure 26. At this point, the degree of superheat and subcooling are 7K and 3K, respectively, and the sight glasses are clear. The blue line represents constant entropy. This operating point is used to validate the model. The experimentally measured and calculated performance metrics are displayed in Table 8. The heat transfer rate of the evaporator is calculated using Equation (4).

$$Capacity = \dot{m}(h_1 - h_4) \quad (4)$$

In order to assure energy balance, the heat transfer rate of the condenser is also needed and is calculated by Equation (5).

$$\dot{Q}_{cond} = \dot{m}(h_2 - h_3) \quad (5)$$

The system's performance is analyzed using COP and isentropic efficiency calculated using Equations (6) and (7).

$$COP = \frac{\dot{m}(h_1 - h_4)}{\dot{W}_{meas}} \quad (6)$$

$$\eta_s = \frac{h_{2,s} - h_1}{\dot{W}_{meas}} \quad (7)$$

Table 8: Sensible Cooling Load Test Metrics

Parameter	Value	Unit
Cooling Capacity	4710	W
\dot{Q}_{cond}	5743	W
\dot{W}_{meas}	957	W
COP	4.92	-
η_s	64.87	%

According to the first law of thermodynamics, the energy input must equal the energy output. For a VCC, the two inputs are heat gained by evaporator and compressor work while the single output is heat rejected by the condenser. Analysis of the energy balance shows a 76 W difference between energy input and output, which is equivalent to an imbalance of 1.32%. This imperfect energy balance can be attributed to not perfectly insulated line sets. In Figure 27, the variable speed compressor dynamics can be seen. Initially, the compressor works at its rated frequency to quickly cool the habitat. Once the habitat is cooled close to the set point, the inverter varies the frequency of the compressor to reduce overshoot and energy losses.

The second test as outlined in Table 6 of Chapter 3 was conducted with a 2500 W sensible heating load and a latent load. The relative humidity was initially 25% at 22°C ($\omega = 0.00409$ kg/kg). The target superheat and subcooling was 10K to assure single phase in order to accurately predict the enthalpies with temperature and pressure. The pressures and temperatures of the VCC state points from Figure 10, Pressure-specific enthalpy (P-h) diagram at steady state, bladder air temperature, and humidity ratio are shown in Figures 28, 29, 30, and 31, respectively.

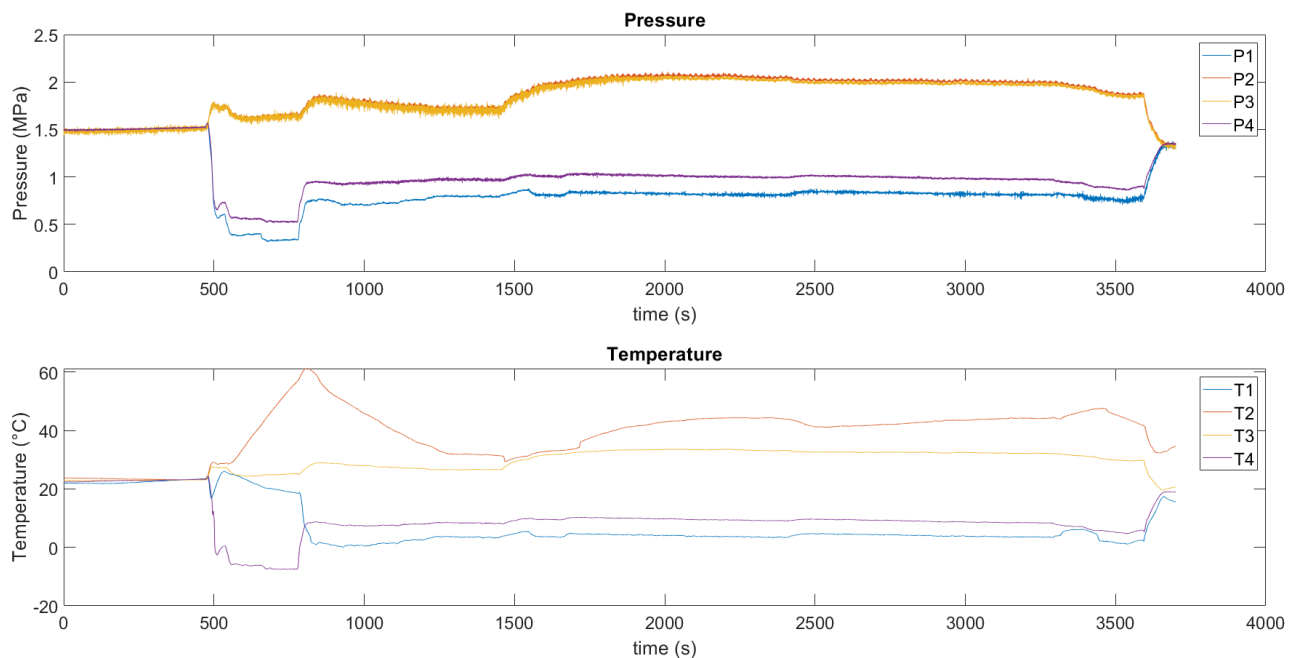


Figure 28: Sensible and Latent Cooling Load Test Pressure and Temperature vs Time at Cycle State Points

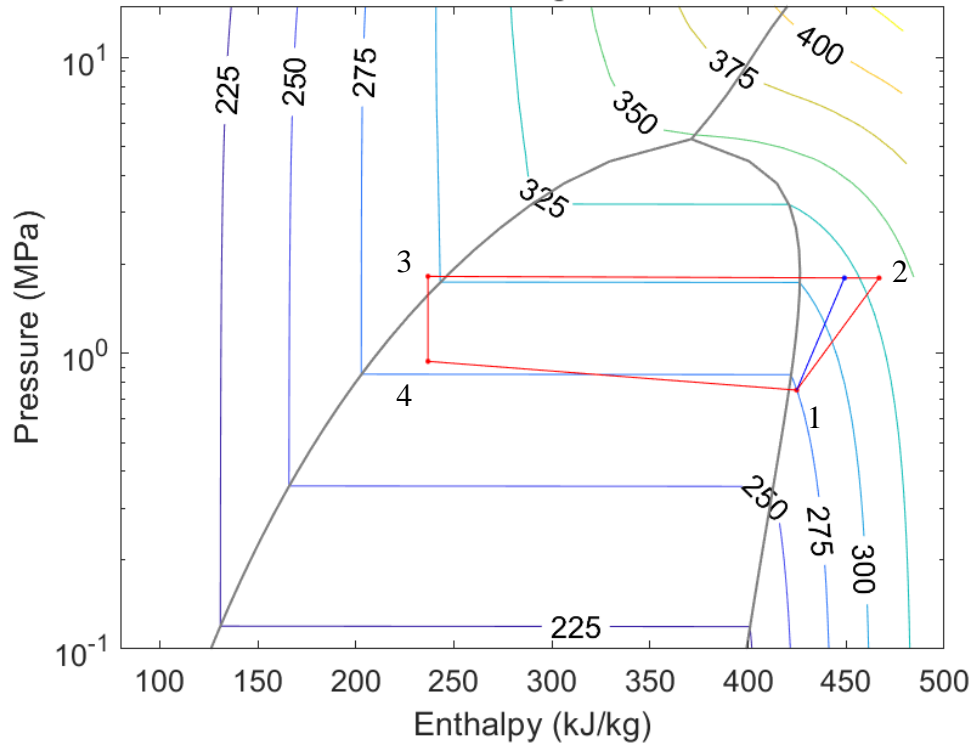


Figure 29: P-h Diagram of Sensible and Latent Cooling Load Test at Steady State

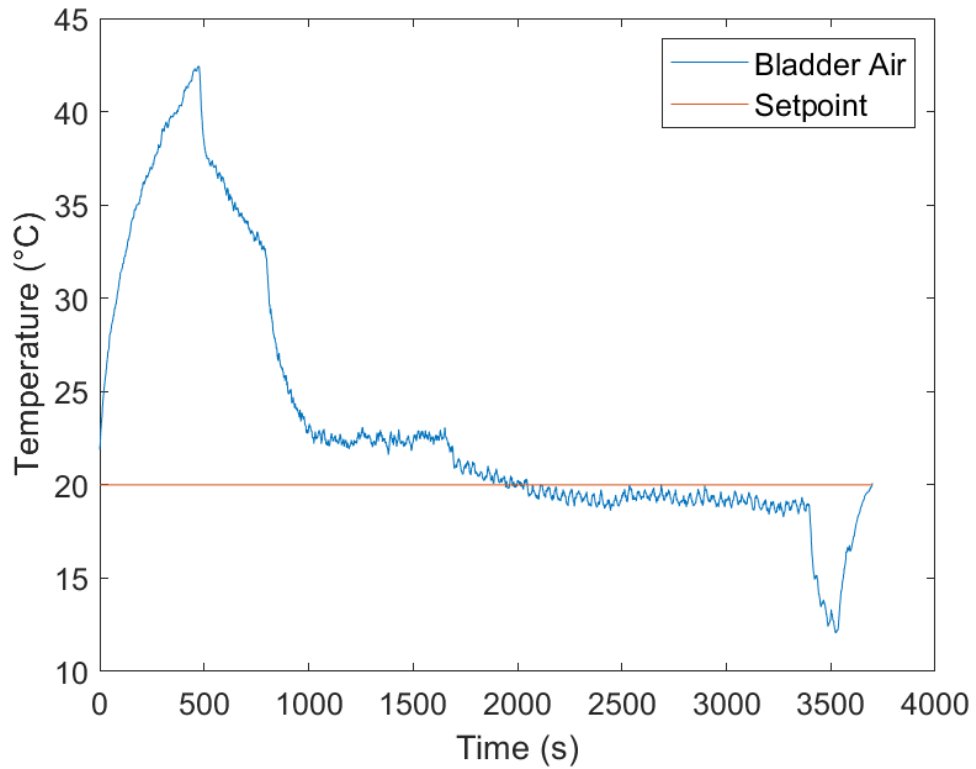


Figure 30: Bladder Air Temperature vs Time: Sensible and Latent Cooling Load Test

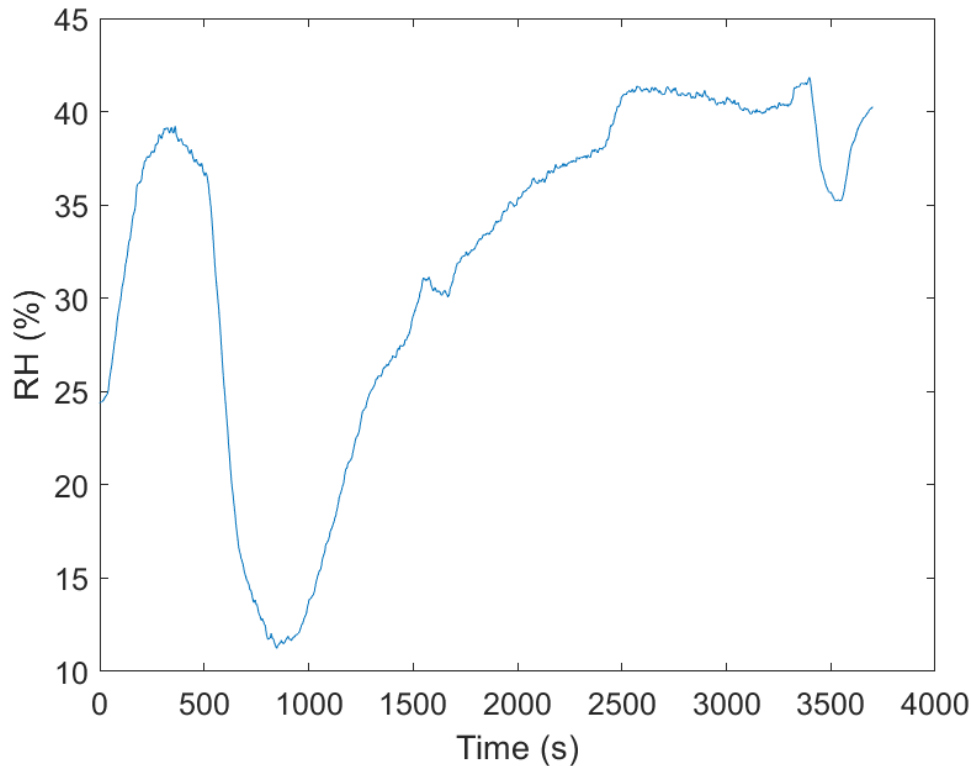


Figure 31: Bladder Relative Humidity vs Time: Sensible and Latent Cooling Load Test

The sensible and latent loads were applied to the habitat at $t = 0$ seconds. The habitat was first allowed to heat up so that the heat pump would reach a steady state operating condition. Before turning the heat pump on, the relative humidity was 39% at 42.5°C ($\omega = 0.02085 \text{ kg/kg}$). As shown in Figure 28, the heat pump was turned on at $t = 470$ seconds. In a similar manner to the first test, the peak represents “steady state”. Again, the compressor floods despite the additional latent load and occurs between $t = 810$ to 1470 seconds. However, at $t = 1716$ seconds, the evaporator fan speed is increased and a noticeable change in the discharge temperature is observed. The increase in fan speed does not entirely solve the flooding problem but lessens the effects. Plotting pressure and enthalpy the instant before the compressor starts to flood results in the P-h diagram shown in Figure 29. At this point, the degree of superheat and subcooling are 10K and 1K, respectively, and the sight glasses are clear. The blue line represents constant entropy. This operating point is used to validate the model. The performance metrics for this test are displayed in Table 9.

Table 9: Sensible and Latent Cooling Load Test Metrics

Parameter	Value	Unit
Cooling Capacity	4956	W
\dot{Q}_{cond}	6052	W
\dot{W}_{meas}	1005	W
COP	4.93	-
η_s	64.85	%

Analysis of the energy balance shows a 91 W difference between energy input and output, which is equivalent to an imbalance of 1.50%. The capacity increases by 245 W from the sensible only test. This 245 W is assumed to be the latent load. Before the unit reaches the setpoint temperature the relative humidity is 41% at 20°C ($\omega = 0.00594$ kg/kg noticeable decrease in humidity ratio). As seen in Figure 30, the unit overshoots the set point which questions the manufacturer controller’s capabilities. The varying of the inverter is not present as it was in the sensible only load test.

4.2.3 Heating Load Results

In order to impose heating load on the habitat, a single thermal transfer panel was used. The first test outlined in Table 7 of Chapter 3 was conducted by setting the chiller’s fluid outlet temperature to -40°C. The heat pump was turned on when the habitat reached 17.5°C and allowed to reach its setpoint temperature. After reaching the setpoint temperature, the heat pump was turned off and the habitat was allowed to cool down in order to characterize the effect of the thermal transfer panel load. The target superheat and subcooling was 10K to assure single phase in order to accurately predict the enthalpies with temperature and pressure. The pressures and temperatures of the VCC state points from Figure 10, P-h diagram at steady state, and bladder air temperature are shown in Figures 32, 33, and 34, respectively.

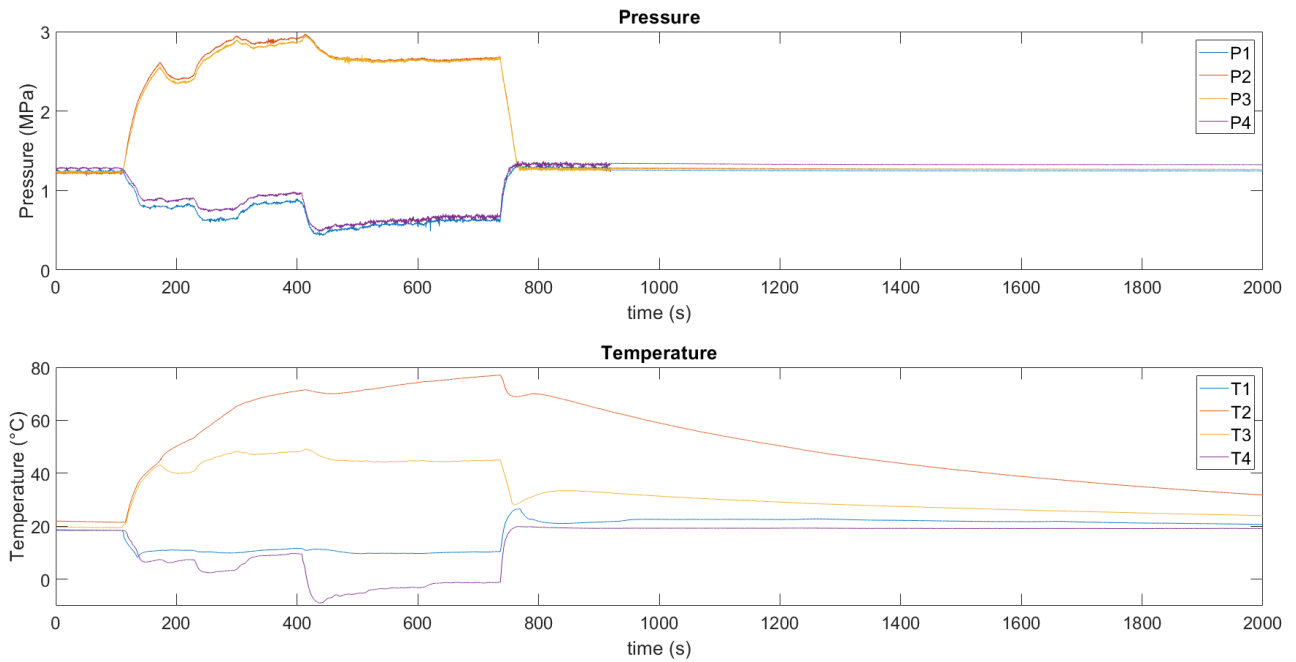


Figure 32: -40°C Panel Temperature Test Pressure and Temperature vs Time at Cycle State Points

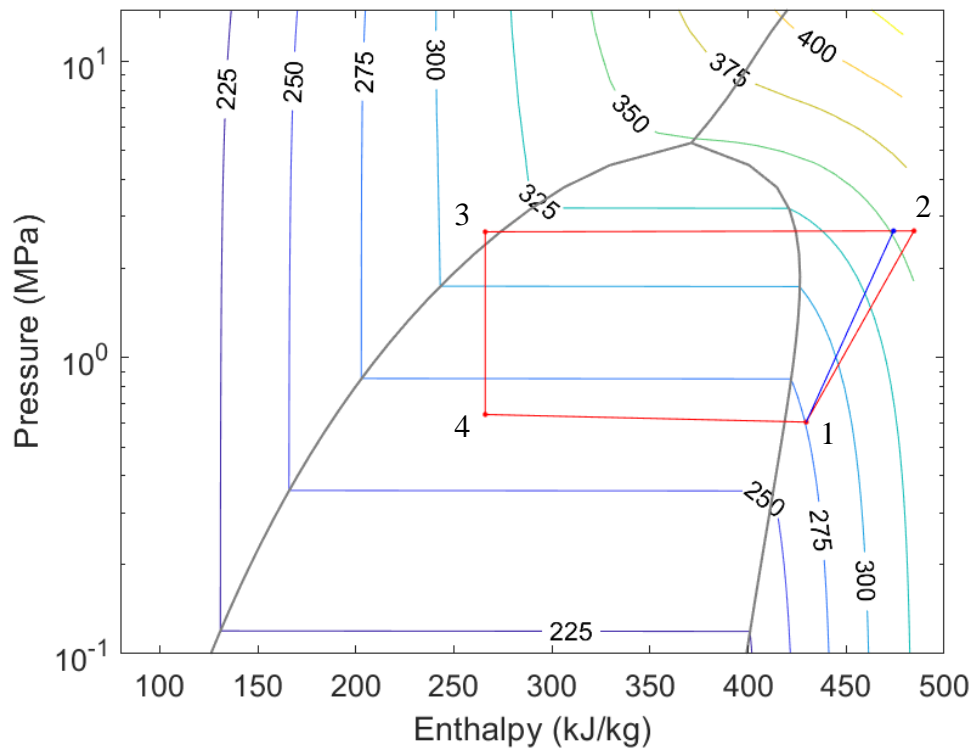


Figure 33: P-h Diagram of -40°C Panel Temperature Test at Steady State

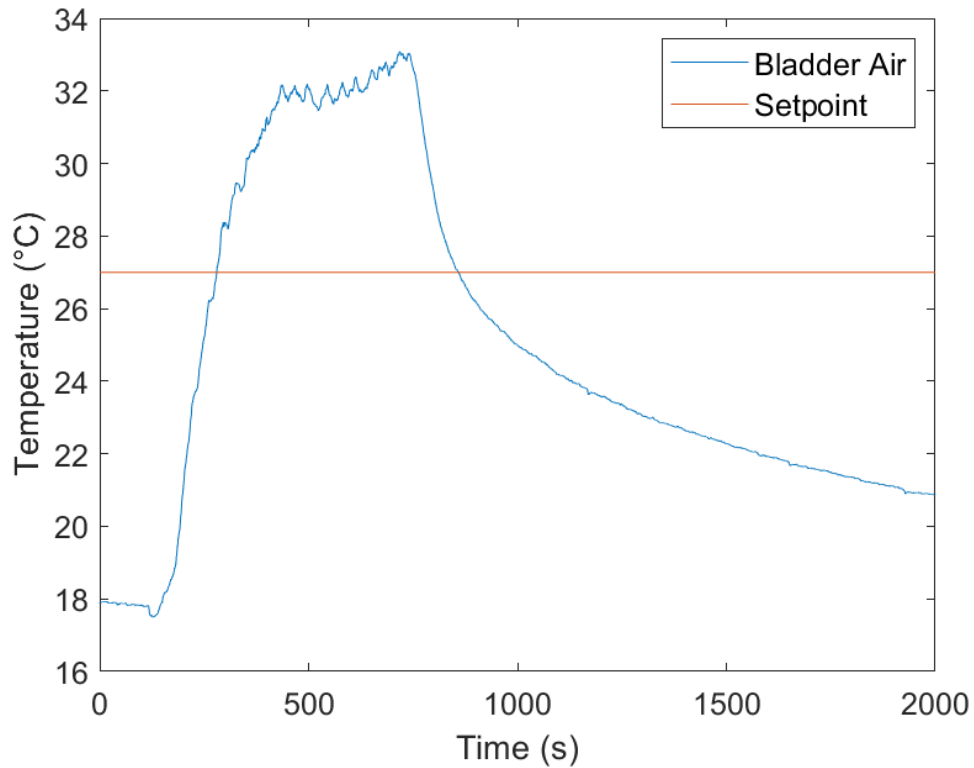


Figure 34: Bladder Air Temperature vs Time -40°C Panel Temperature Test

The heat pump achieves a steady state condition at $t = 736$ seconds as seen in Figure 32. Plotting pressure and enthalpy at this time results in the P-h diagram shown in Figure 33. At this point the superheat is 10K, the subcooling is 3K, and the sight glasses are clear. This operating point is used to validate the model. After $t = 736$ seconds, the heat pump reaches the setpoint temperature and turns off. Unlike the cooling tests, the heat pump does not flood and start slugging. It can be seen that the cycle operates at a relatively steady condition for about 300 seconds prior to reaching the setpoint. As displayed in Figure 34, at a panel temperature of -40°C, the habitat does not experience a large temperature drop with respect to time. At the steady state operating condition, the performance metrics were measured and calculated. The results are displayed in Table 10.

Table 10: -40°C Panel Temperature Test Metrics

Parameter	Value	Unit
Heating Capacity	2120	W
\dot{Q}_{evap}	1587	W
\dot{W}_{meas}	816	W
COP	2.60	-
η_s	81.04	%

Analysis of the energy balance shows a 283 W difference between energy input and output, which is equivalent to an imbalance of 13.34%. Similarly, a high isentropic efficiency is calculated. The imperfect insulation of the line sets explains this imbalance. The effects of heat loss are amplified more in heating mode than in cooling mode due to where the discharge temperature is measured. In both cooling and heating mode, the discharge temperature is measured at the inlet of the condenser. The problem with heating mode is that the condenser is roughly 4.5 meters away from the compressor due to it being located inside of the habitat. The desuperheating occurring in the line sets is not captured by data acquisition. In summary, the discharge temperature measured is lower than expected leading to an inaccurate prediction of the enthalpy at state point two.

The second test outlined in Table 7 of Chapter 3 was conducted by setting the chiller’s fluid outlet temperature to -60°C. The heat pump was turned on when the habitat was at 18.5°C and allowed to reach its setpoint temperature. After reaching the setpoint temperature, the heat pump was turned off and the habitat was allowed to cool down in order to characterize the effect of the thermal transfer panel load. The target superheat and subcooling was 10K to assure single phase in order to accurately predict the enthalpies with temperature and pressure. The pressures and temperatures of the VCC state points from Figure 10, P-h diagram at steady state, and bladder air temperature are shown in Figures 35, 36, and 37, respectively.

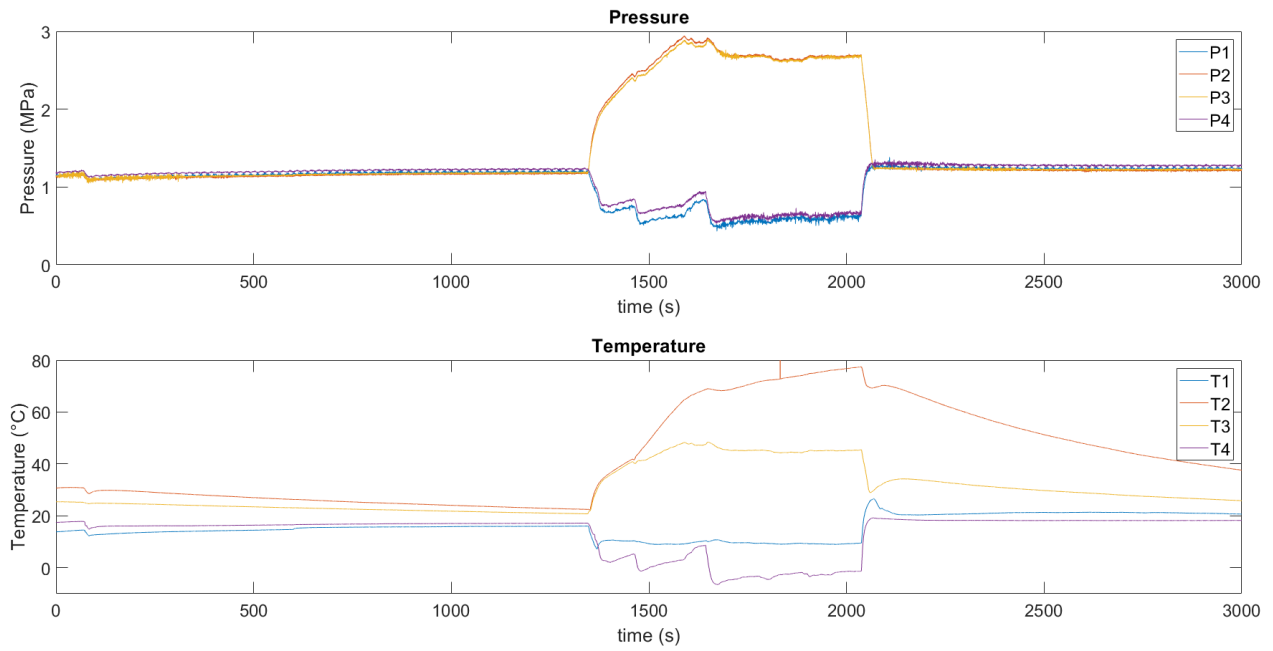


Figure 35: -60°C Panel Temperature Test Pressure and Temperature vs Time at Cycle State Points

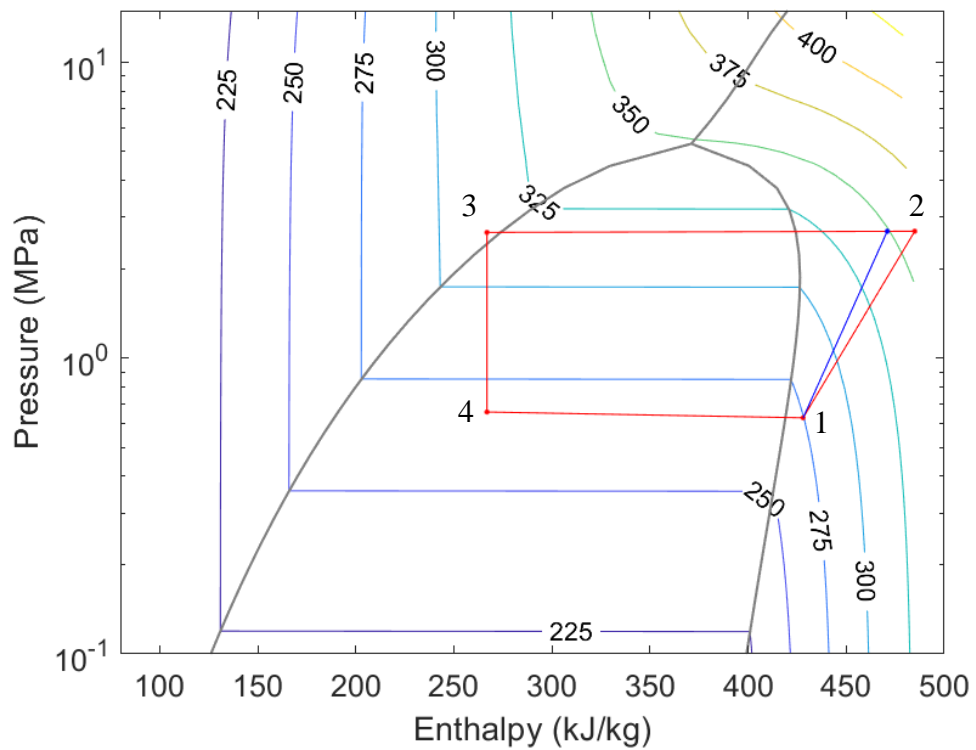


Figure 36: P-h Diagram of -60°C Panel Temperature Test at Steady State

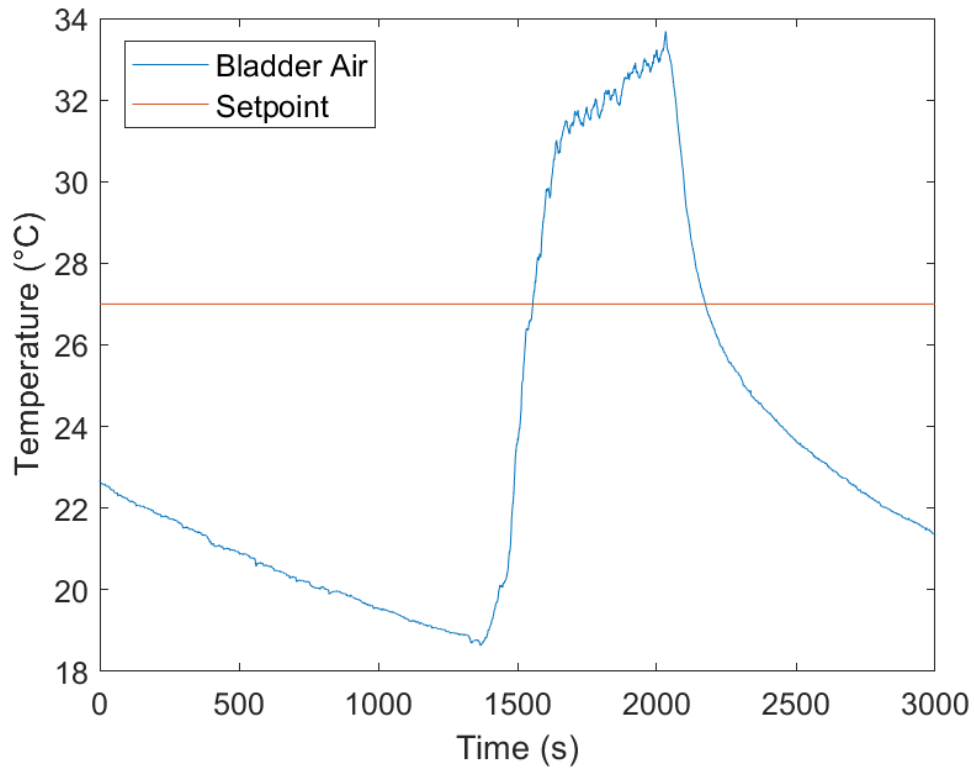


Figure 37: Bladder Air Temperature vs Time -60°C Panel Temperature Test

The heat pump reaches a steady state operating condition at $t = 2036$ seconds as seen in Figure 35. Plotting pressure and enthalpy at this time results in the P-h diagram shown in Figure 36. At this point the superheat is 8K, the subcooling is 3K, and the sight glasses are clear. This operating point is used to validate the model. After $t = 2036$ seconds, the heat pump reaches the setpoint temperature and turns off. It can be seen that the cycle operates at a relatively steady condition for about 350 seconds prior to reaching the setpoint. As displayed in Figure 37, at a panel temperature of -60°C , the habitat experiences a larger temperature drop with respect to time as compared to the test with the panel temperature at -40°C . At the steady state operating condition, the performance metrics were measured and calculated. The results are displayed in Table 11.

Table 11: -60 °C Panel Temperature Test Metrics

Parameter	Value	Unit
Heating Capacity	2198	W
\dot{Q}_{evap}	1624	W
\dot{W}_{meas}	838	W
COP	2.62	-
η_s	75.38	%

Analysis of the energy balance shows a 264 W difference between energy input and output, which is equivalent to an imbalance of 12.01%. Similarly, a high isentropic efficiency is calculated. As the previous tests, the imperfect insulation of the line sets explains this imbalance.

4.3 Discussion

The instabilities present when operating in cooling mode suggest that the heat pump is oversized for the current loads. Characterizing these instabilities proved to be very difficult with the limited control of the equipment and the data that was acquired. A very large pressure drop between the inlet and outlet of the indoor heat exchanger during cooling mode was recorded. It can also be seen in Figures 25 and 28 that after the compressor starts to flood, the outlet of the evaporator is a lower temperature than the inlet. This behavior alludes to the refrigerant expanding twice: at the expansion valve and somewhere within the evaporator coil. A conclusion can be made about the systems instabilities in cooling mode: the small volume of the habitat and the position of the indoor unit leads to limited air circulation. The indoor unit's air outlet is located near the floor of the habitat. The cold, conditioned air is denser than the hot air that the unit's thermostat is reading. This suggests that the cold air and hot air are separated and never mix. This stable, no flow condition, means there is essentially no heat transfer between the hot air read by the thermostat and the refrigerant.

In heating mode, the difference in load between the -40°C panel temperature and the -60°C panel temperature is around 100 W. The data shows that the heat pump operating conditions— T_{evap} , T_{cond} , and compressor speed—are nearly identical for the two tests. This suggests that a large

thermal resistance exists between habitat air and the thermal transfer panel that restricts heat flow out of the system. In order to assure maximum heat transfer from the habitat to the panel the bladder must be in constant contact with the panel. To achieve this, the bladder is inflated with compressed air. The compressed air infiltrates the habitat at ambient temperature. Despite the infiltration load not being characterized by experimental data, it can be assumed that some of the heat balances the load provided by the single panel. There were no instabilities present in heating mode. This can be attributed to proper air circulation due to the less dense, hot air leaving the indoor unit mixes with the denser cold air.

4.4 Model Validation

The model, as outlined in Chapter 2, is to be validated with experimental data. Experimentally measured indoor and outdoor temperatures as well as superheat and subcooling will be inputted into the model. The model will output T_{evap} , T_{cond} , capacity, and power consumption. The outputs will then be directly compared to experimentally measured values. Figures 38 and 39 show the results of comparing the semi-empirical model to the experimental data.

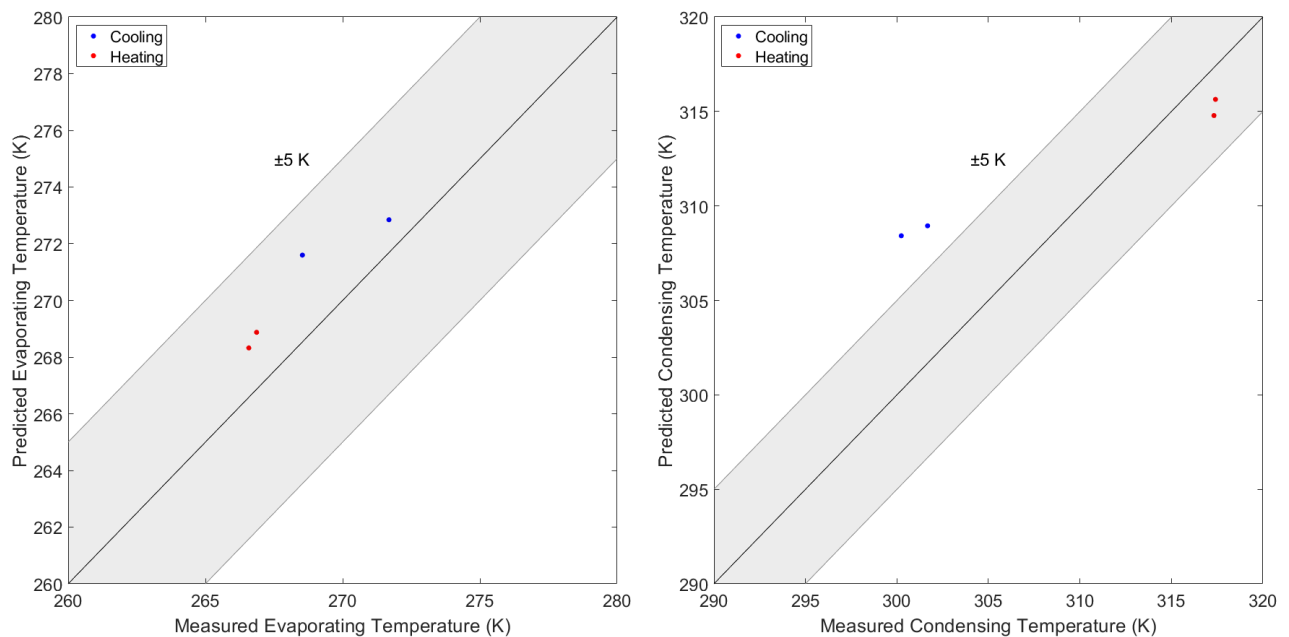


Figure 38: Measured vs Predicted Evaporating Temperature (left) and Condensing Temperature (right)

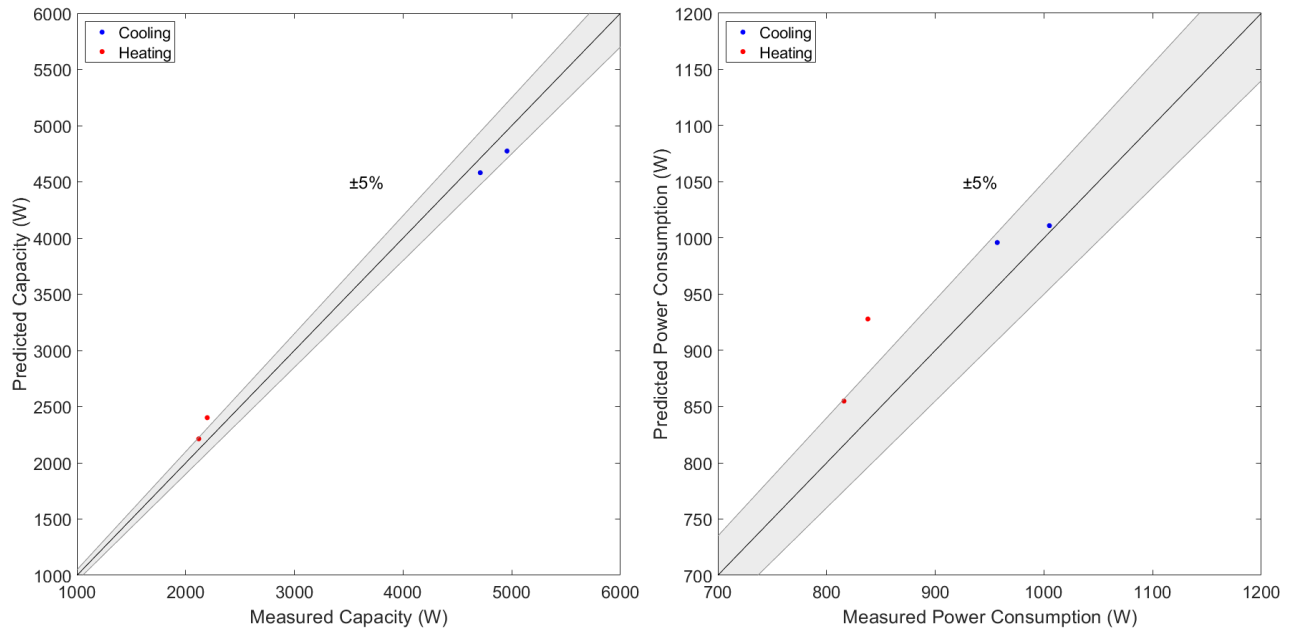


Figure 39: Measured vs Predicted Capacity (left) and Power Consumption (right)

Figure 38 shows the measured versus predicted values of evaporating and condensing temperatures for the four steady state data points recorded. The model, in its current form, is able to accurately predict the evaporating temperature within ± 5 K for both heating and cooling modes. On the other hand, the model is not able to accurately predict the condensing temperature in cooling mode. Figure 39 shows the measured versus predicted values of capacity and power consumption for the four steady state data points recorded. The capacity and power consumption in heating mode are slightly over predicted whereas in cooling mode are accurately predicted within $\pm 5\%$. Overall, the model performs well for the data points evaluated. Due to the many assumptions made during the modeling process, it may need to be tuned to make better predictions. At this point, tuning was not performed due to the small size of the data set. Ideally, the model would be tuned with more data points over a large range in order to fully optimize the model.

5. PARAMETRIC STUDY

5.1 Motivation

RETHi's goal is not to design an extra-terrestrial habitat but rather answer difficult research questions, develop models, methods and prototypes that are resilient to deep space disturbances, and conduct experiments to validate computational work. In order to give insight on commissioning a deep space environmental control system, parametric studies will be performed using the model developed in Chapter 2. The model will be used to optimize and scale the sizing of the heat pump components for a variety of scenarios. The parametric studies also aim to predict the system's response given its requirements for the CPT. Since the CPT is pressurized above one atmosphere, psychometrics will change when analyzing latent loads. These results will be particularly versatile as they can be applied to other closed pressurized environments. Conversely, in a deep space habitat, day variations and loads will contribute to different environmental control system requirements. To study these different thermal management requirements, the heat pump cycle model will be coupled with the IE model [33].

5.2 No Disturbance Load Calculations

Thermal loading and unloading of the deep space habitat cannot be overlooked when sizing the HVAC system. During no disturbance scenarios, the habitat will need to be cooled and dehumidified. This is due to the many factors that generate heat within the IE. Internal heat gains such as people, lighting, appliances, and electronics will contribute to the cooling load. ASHRAE provides extensive data for calculating building heat loads. Table 8 shows the rates at which heat and moisture are produced by humans and Table 9 shows the rates heat produced by a variety of electric devices applicable to a deep space habitat. For simplification purposes in calculating heat loads, only the most common electronics were selected.

Table 12: Human Heat and Moisture Rates (Adapted from [34])

Activity	Sensible Heat (W)	Latent Heat (W)
Seated (Sleeping)	70	35
Moderately active office work	75	55
Heavy Work	170	255

Table 13: Heat Rates by Electronic Devices (Adapted from [34])

Source	Rate of Heat Gain (W)
Laboratory Lighting	83
Microwave Oven	1141
Average of Typical Laboratory Equipment	204
High Performance Desktop Computer	151
LED Monitor	50
Fridge	387

Unlike a terrestrial building, windows and insulation play less of a role in an extraterrestrial habitat. As outlined in [35] and implemented in the structural protective layer model, the outside of the habitat is to be insulated with lunar regolith. Lunar regolith has great insulation thermophysical properties as outlined in Table 10.

Table 14: Regolith Thermophysical Properties (Adapted from [36])

Property	Value	Unit
Emissivity	0.97	-
Density	2000	kg/m ³
Thermal Conductivity	0.014	W/m-K
Specific Heat Capacity	1053	J/kg-K

Studies performed by the modeling team have shown that the extreme temperature variations of the Moon have little impact on the heat gain/loss of the habitat. Figure 40 shows a plot of the temperature at different depths of the structural protective layer. The bottom temperature measurement, which is closest to the habitat wall, shows very little variation in temperature which leads to minimal heat gains/losses seen by the interior environment. Due to the very low thermal conductivity of regolith and sufficient thickness it acts as a great insulator to the harsh temperatures of the Moon.

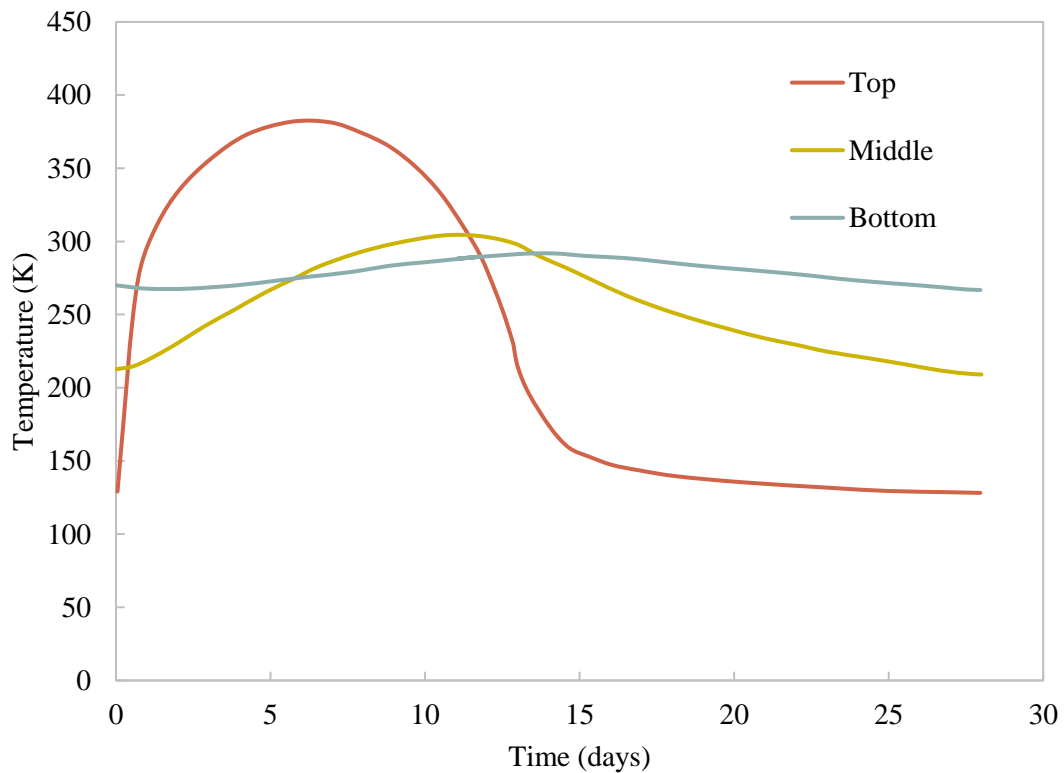


Figure 40: Temperature at Various Depths of the Structural Protective Layer vs Time (Adapted from [36])

In order to study the effects of loading and unloading, a load profile was developed. The load profile in Figure 41 follows the subsequent reasonable assumptions:

- Total number of crew members is 8 based on 0.57 m³ volume of habitat per crew member [35]
- Crew members sleep for 8 hours
- Half of the crew works moderately performing office work for 8 hours
- Half of the crew works heavily for 8 hours
- During non-working and non-sleeping hours crew members are sitting
- Lights are on for 16 hours
- All electronics are in low power mode during non-working hours
- Microwave oven is operated three times a day for breakfast, lunch and dinner
- Refrigerator operates continuously
- All latent loads from showering are exhausted completely and do not contribute to the cooling load.

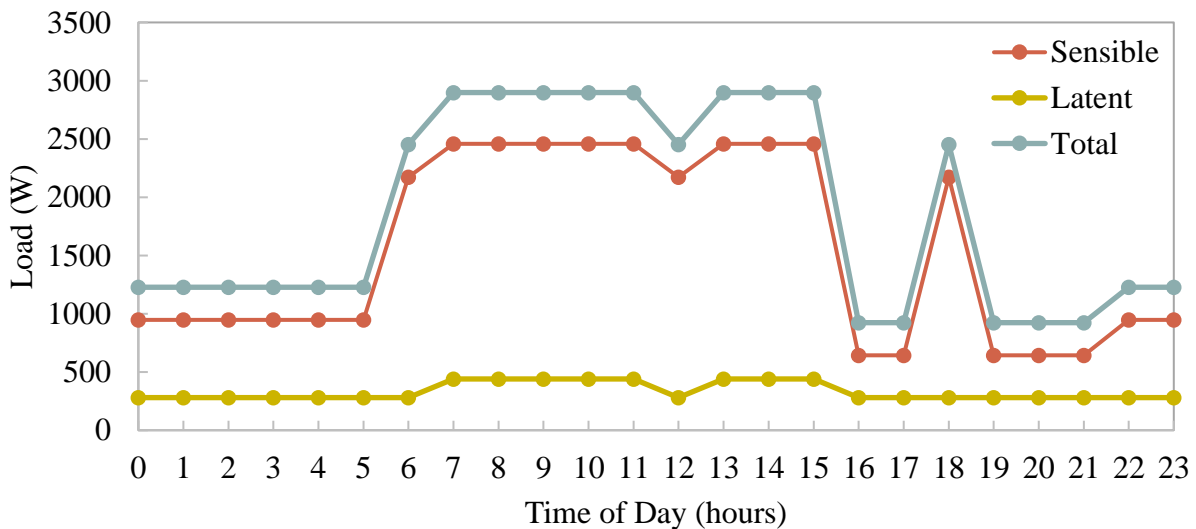


Figure 41: Load Profile Developed for Studying HVAC System Requirements and Response

5.3 Thermal Transfer Panel Load Calculations

Thermal transfer panels are to be used to simulate damage to the structural protective layer. During a meteorite impact, the regolith layer will be damaged leading to thinning or total loss of insulation. This will expose the habitat wall to the extreme temperatures of the Moon. Without insulation, heat will be lost or gained due to the large temperature difference between the IE and habitat wall. In order to estimate the heat loss when the thermal transfer panel is set below the ambient temperature of the IE, Equation (8) will be used [37] to predict the free convection heat transfer coefficient. Since the dimensions of the thermal transfer panel are known, the following assumptions will be made: vertical flat plate, uniform temperature, fully insulated back side, IE air is an ideal gas and the air is quiescent.

$$\overline{Nu} = \left\{ 0.825 + \frac{0.387Ra_{\bar{\delta}}^{\frac{1}{4}}}{\left[1 + \left(\frac{0.492}{Pr} \right)^{\frac{9}{16}} \right]^{\frac{8}{27}}} \right\}^2 \quad (8)$$

Assuming all nine panels are turned on, inputting the minimum chiller fluid outlet temperature of -70°C and taking the ambient temperature of the IE to be 25°C results in a maximum load of -4330 W.

5.4 Results and Discussion

In order to characterize the heat pump's performance, the model was used to predict the capacity with varying evaporating temperatures, condensing temperatures and compressor speeds. Evaporating temperature varies from -10°C to 20°C. Condensing temperature varies from 40°C to 60°C. Figures 42, 43, and 44 display predicted capacity at minimum compressor speed, intermediate compressor speed and rated compressor speed respectively. The minimum compressor speed is 30 Hz. Intermediate compressor speed is defined by Equation 9 and found to be 40 Hz. The rated compressor speed is 60 Hz.

$$Intermediate\ Hz = \frac{Rated\ Hz - Minimum\ Hz}{3} + Minimum\ Hz \quad (9)$$

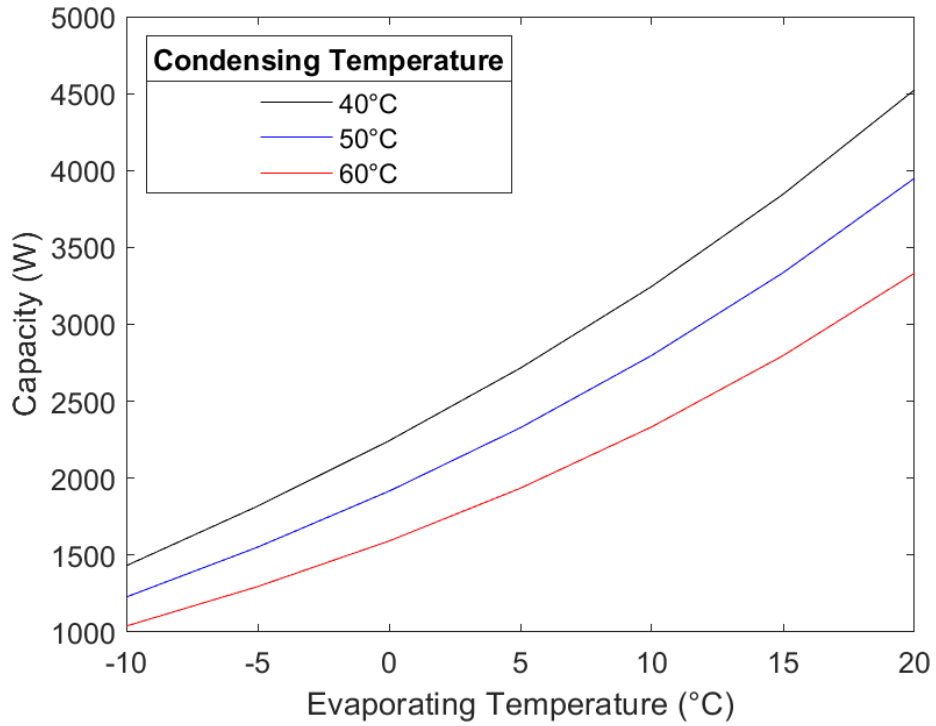


Figure 42: Capacity as a Function of Evaporating and Condensing Temperature at Minimum Compressor Speed

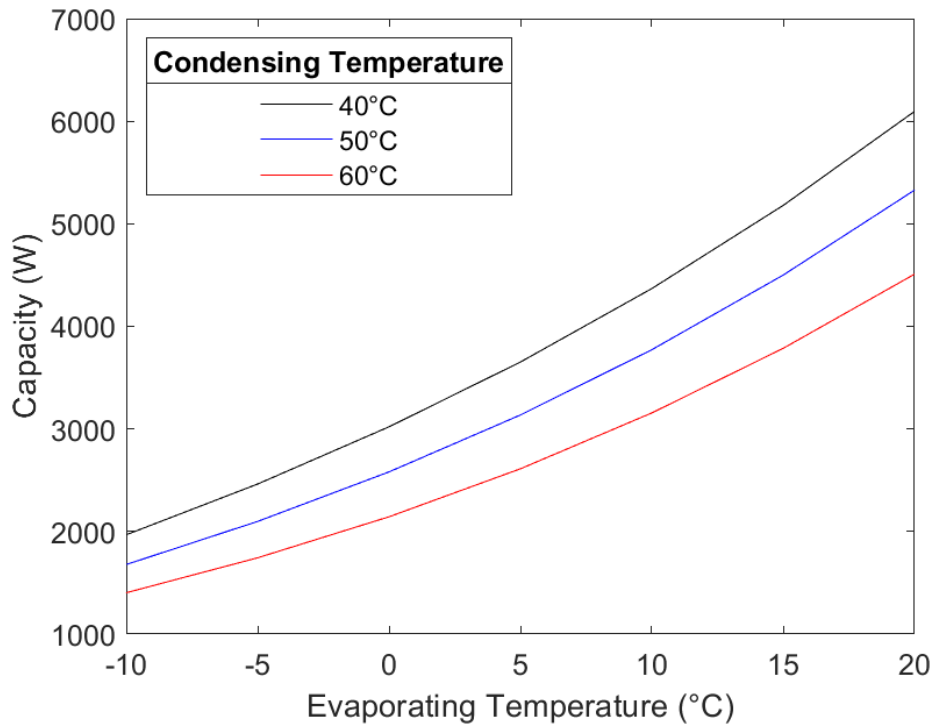


Figure 43: Capacity as a Function of Evaporating and Condensing Temperature at Intermediate Compressor Speed

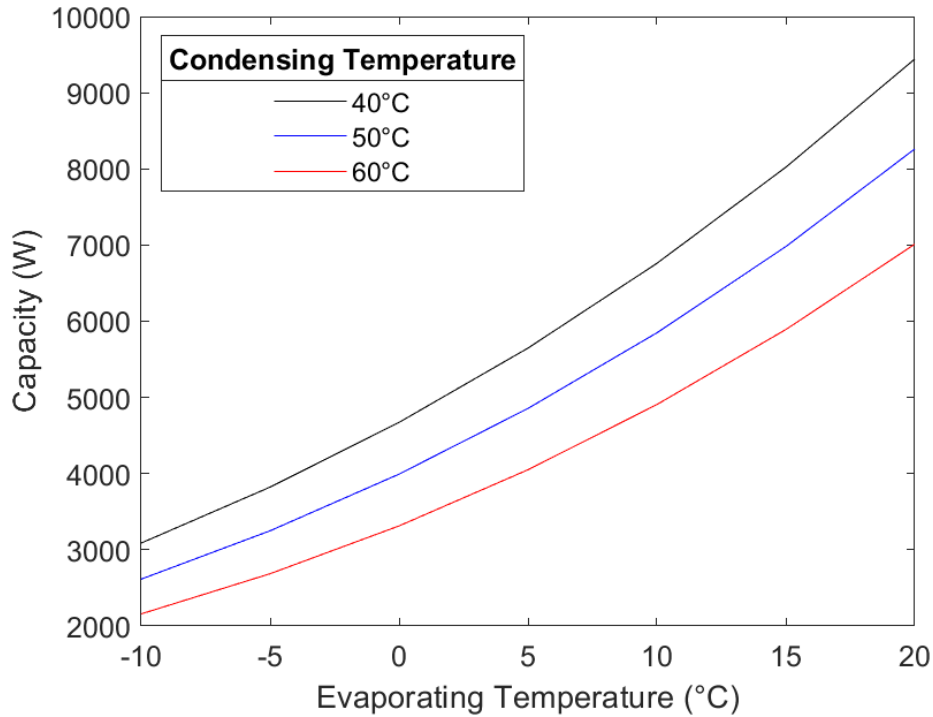


Figure 44: Capacity as a Function of Evaporating and Condensing Temperature at Rated Compressor Speed

As shown in Figures 42, 43, and 44, as the evaporating temperature and compressor speed increase, so does capacity. At a fixed condensing temperature and subcooling, the lower the evaporating temperature, the higher the quality of refrigerant at the outlet of the expansion valve. This leads to a smaller enthalpy difference across the evaporator. Similarly, at higher compressor speeds mass flow increases leading to a higher capacity. On the other hand, as condensing temperature increases, capacity decreases. With a fixed subcooling, this is as expected since the enthalpy at the outlet of the condenser decreases with increasing condensing temperature.

The superposition of the IE load and heat pump capacity would illustrate the system requirements versus system response. In order to capture this behavior, five case studies were performed by coupling the IE model developed by [33] with the heat pump model. The air temperature results from *Cooling Test One* was compared to the coupled model as displayed in Figure 45. Overall, the model is in good agreement with the experimental data.

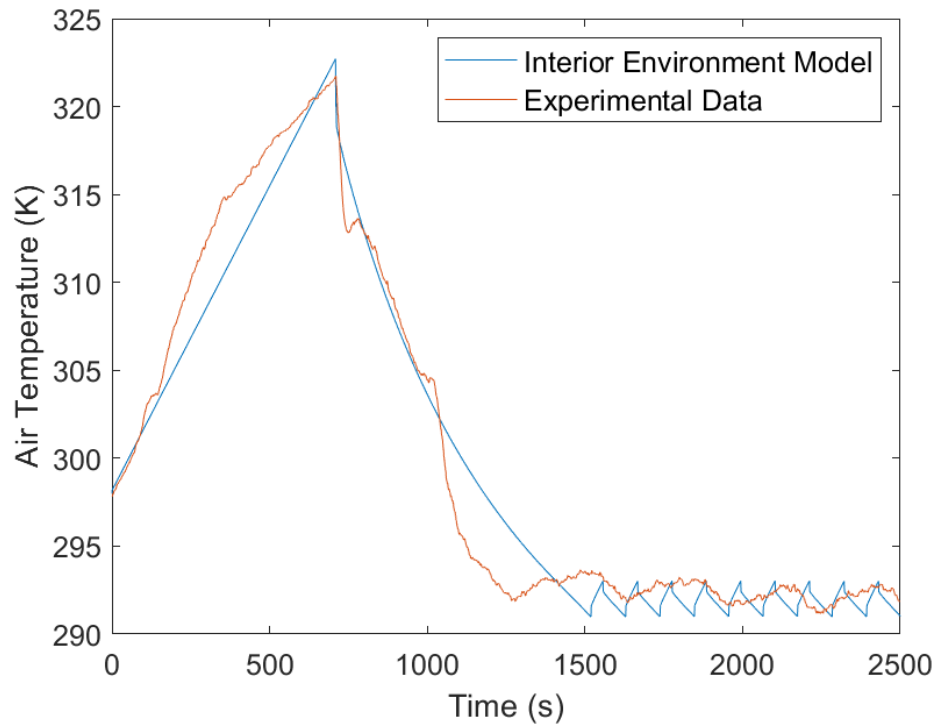


Figure 45: Validation of IE Model Air Temperature vs Time

The first two case studies, displayed in Figures 46 and 47, investigate the minimum and maximum cooling loads, respectively, of the profile developed in Section 5.2.1. The third case study, displayed in Figure 48, investigates the maximum heating load imposed by the thermal transfer panels from the calculation in Section 5.2.2. The last two case studies, displayed in Figures 49 and 50, investigate the limits of the heat pump. All case studies were performed for 3600 seconds at rated compressor speed with an outdoor temperature of 25°C, an indoor setpoint temperature of 22°C, subcooling and superheat of 5K.

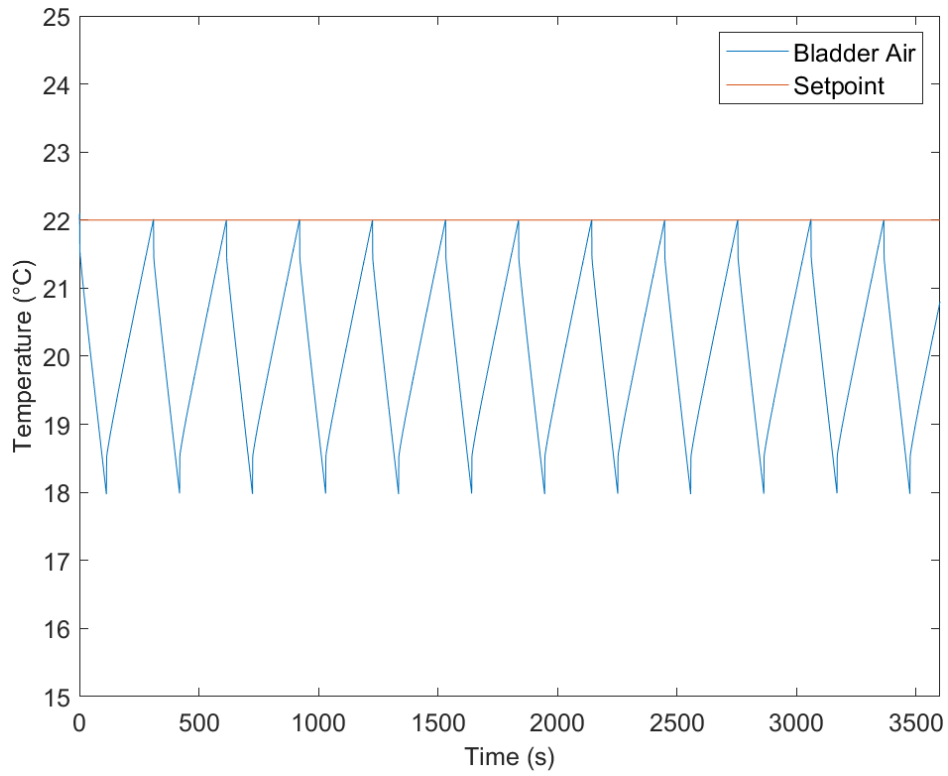


Figure 46: Load of 1227 W IE Air Temperature vs Time

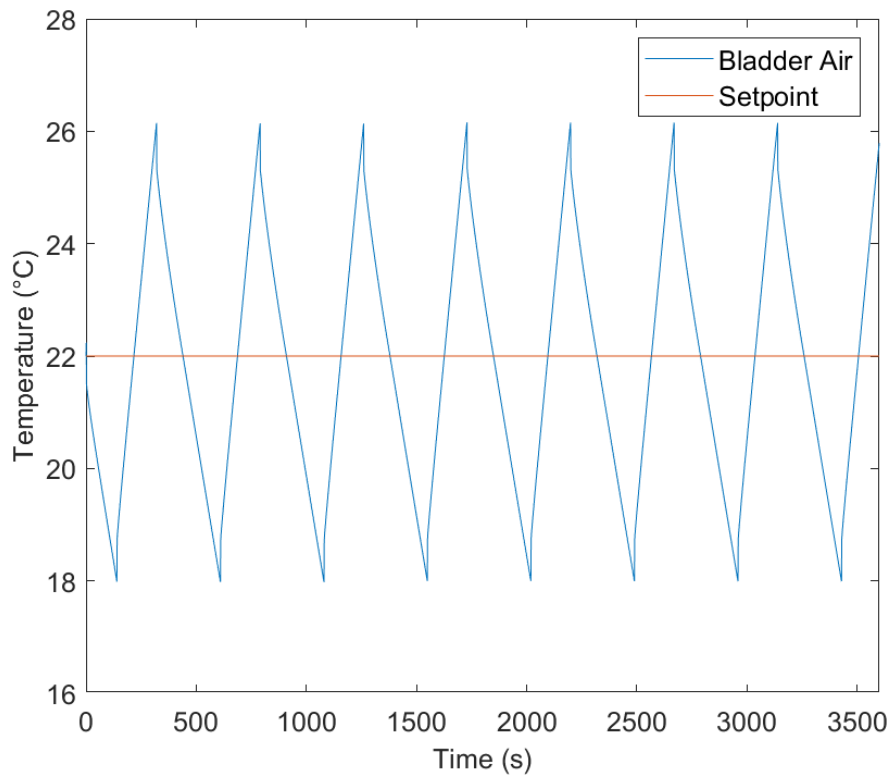


Figure 47: Load of 2898 W IE Air Temperature vs Time

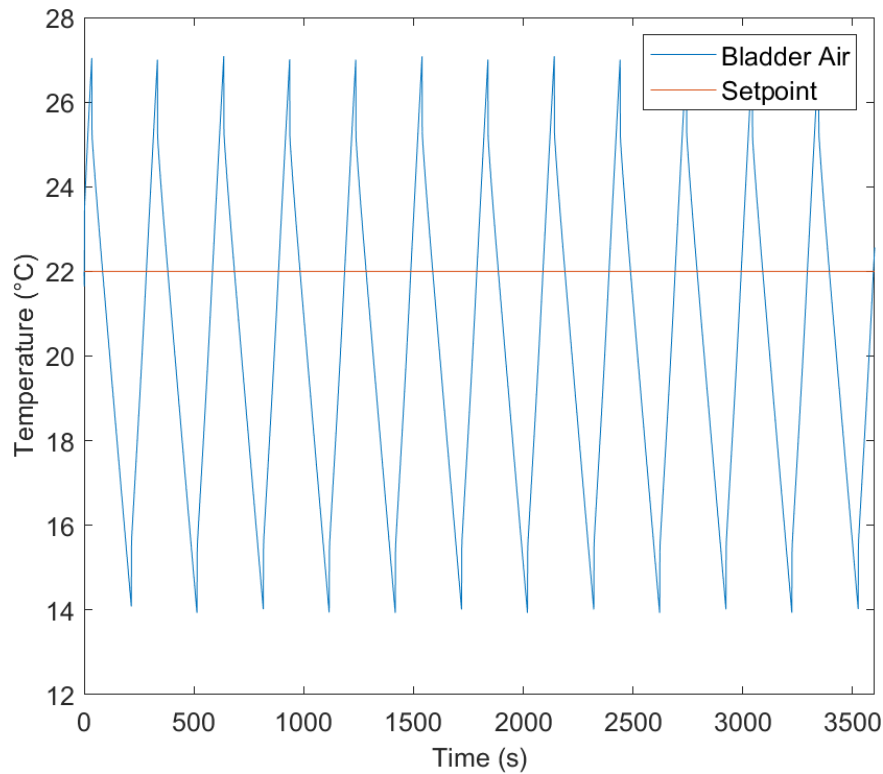


Figure 48: Load of -4330 W IE Air Temperature vs Time

Figure 46 displays the minimum load, 1227 W, experienced by the habitat according to the load profile. As shown in the plot of air temperature with respect to time, the unit shows cyclic behavior. This is due to the load of the habitat being less than the capacity of the heat pump. The heat pump turns on and decreases the temperature of the habitat. The heat pump overshoots the setpoint and turns off. The habitat heats back up due to the 1227 W heat load and it continues to cycle throughout the entire hour of minimum load. Figure 47 displays the maximum load, 2898 W, experienced by the habitat according to the load profile. Again, cyclic behavior is observed. Due to the increase load, less cycles are observed as it takes longer for the heat pump to overshoot the setpoint. Figure 48 displays the maximum load, -4330 W, imposed by the thermal transfer panels. The load is negative due to heat loss; the heat pump operates in heating mode. As shown in the plot, cyclic behavior still persists. The effects of the three-minute compressor protection are present as seen by how quickly the habitat cools down. Within the three minutes the heat pump is unable to turn on, the IE temperature reaches 14.5°C.

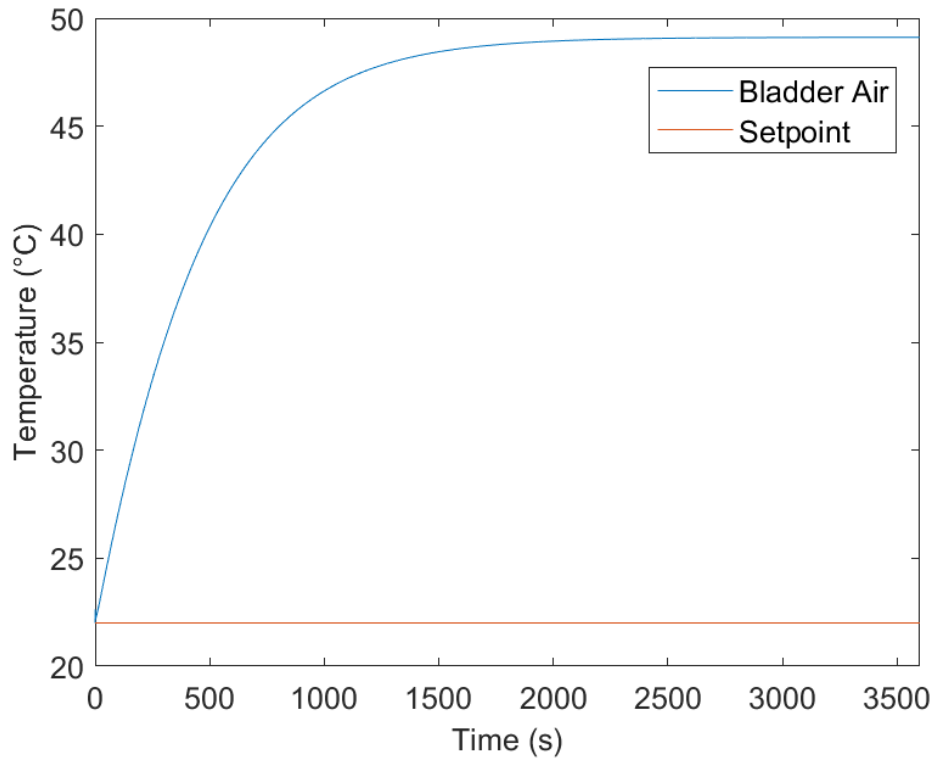


Figure 49: Load of 7500 W IE Air Temperature vs Time

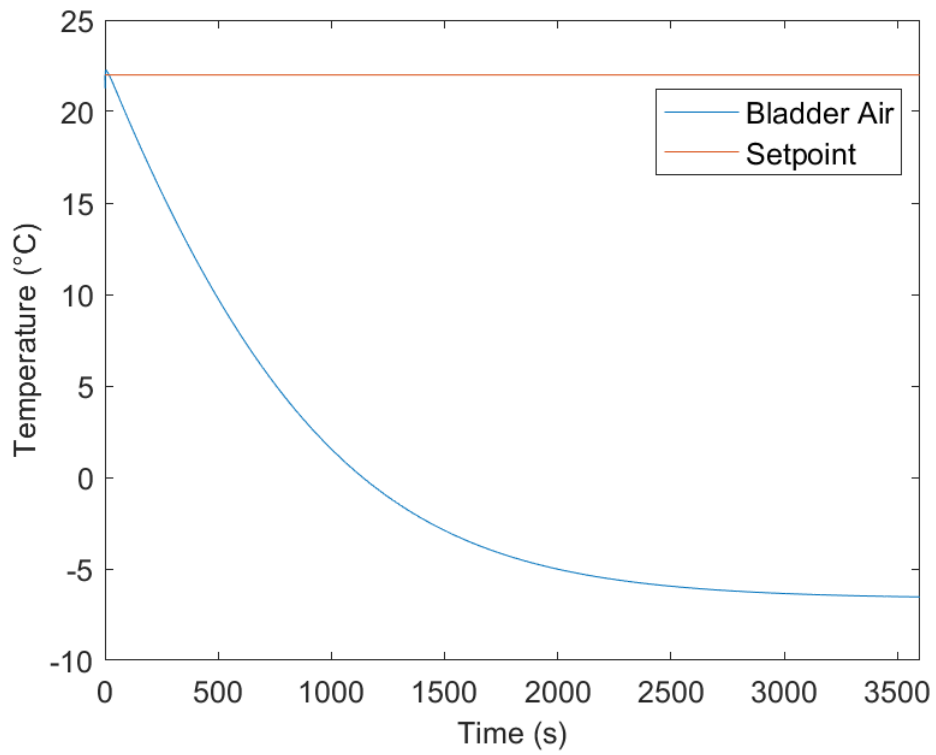


Figure 50: Load of -9000 W IE Air Temperature vs Time

Figure 4

Figures 49 and 50 display the limits of the heat pump at the operating conditions. As shown in 9, the heat pump is unable to maintain the setpoint with a load of 7500 W despite running continuously. A similar behavior is shown for the heating mode case. With a load of -9000 W, the heat pump is unable to maintain the setpoint and results in a substantial decrease in temperature.

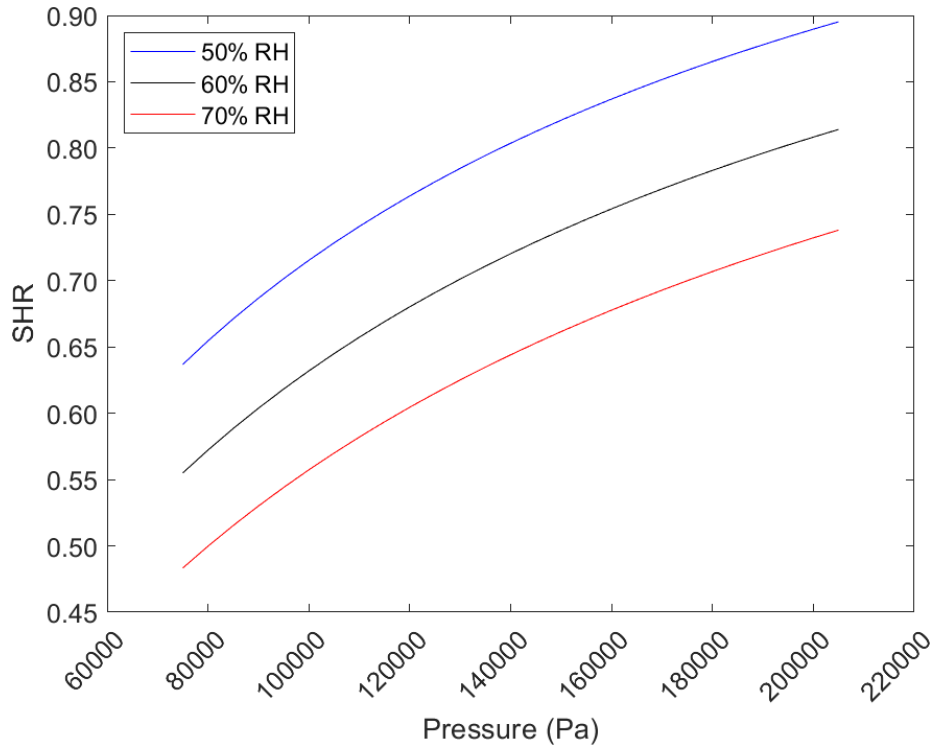


Figure 51: Sensible Heat Ratio vs Pressure at Different Relative Humidities

The last case study analyses the effects of psychrometric on the closed, pressurized environment. In order to study these effects, pressure was varied from 75000 Pa to 202000 Pa and sensible heat ratio (SHR) was analyzed at different relative humidities. SHR is calculated in Equation 10 below.

$$SHR = \frac{\dot{Q}_{sensible}}{\dot{Q}_{sensible} + \dot{Q}_{latent}} \quad (10)$$

75 kPa was chosen as the lower bound as below this pressure humans start to experience psychological problems due to lack of oxygen; 202 kPa was chosen as the upper bound as it is twice the standard atmospheric pressure of 101.325 kPa. As shown in Figure 51, as pressure is

decreased, the effects of dehumidification are amplified. At 75 kPa and 70% RH, more than 50% of the load experienced by the evaporator is used to dehumidify the air. This suggests that evaporators must be sized properly in the event of pressure loss. An evaporator sized for atmospheric pressure will underperform in the event of pressure loss resulting in a less effective sensible heat transfer. This means it will take substantially longer for the heat pump to reach the setpoint temperature.

6. CONCLUSIONS AND FUTURE WORK

6.1 Conclusions and Challenges

This thesis aimed to contribute to numerical and experimental research concerning environmental control systems of resilient extra-terrestrial habitats. The scope of this work consisted of developing a model of the Mitsubishi mini-split system using analytical and empirical methods. The model uses fundamental heat transfer and thermodynamics coupled with real components to analyze the heat pump system. The model accepts indoor temperature, outdoor temperature, wet bulb temperature, superheat and subcooling in order to predict the capacity, power consumption and outlet air conditions. The model was then validated with a small dataset of experiments. Due to the lack of heat loads and thermal transfer panels, the number of possible test cases were very limited. After assuring the model accurately predicted the capacity and dehumidification, the heat pump model was coupled with the IE model. Parametric studies were conducted with the coupled model in order to understand the heat pumps response to the systems requirements. The experimental results and parametric studies suggest that the current heat pump is sized properly for a variety of disturbance scenarios. The ambient temperature of the laboratory, where the outdoor unit resides, results in low condensing temperatures which ultimately lead to capacities above the rating. The model proves to be versatile for not only deep-space habitats but also other closed, pressurized environments such as aircraft and clean rooms.

Commissioning the heat pump to the CPT came with many challenges. At the current state of the project, performing experiments in order to validate the model proved to be quite difficult. Achieving a steady-state condition was arguably not achieved due to insufficient loads and lack of control of the unit. There was also minimal control over the conditions of the IE. Typically, steady-state performance testing is conducted in a well-controlled psychrometric chamber. The consequence of using a purchased mini-split system is that there are many unknowns. For example, the logic of the control board is unspecified and it is unattainable without massive deconstruction and reverse engineering. Similarly, the mini-split system is not controllable. The compressor speed and EXV cannot be adjusted to achieve a steady state condition. Operating the unit under conditions that it was not designed for lead to many instabilities as seen by the compressor flooding and evaporator behavior in cooling mode.

6.2 Future Work

The work outlined in this thesis essentially laid the groundwork for future ECLSS and IE experimentation and modeling. RETHi still has many disturbances and scenarios to investigate. Future scenarios to be tested are power failures, component failures and refrigerant leaks. Since the sizing and capacity requirements were verified with the purchased unit, future work should focus on designing a test stand for the CPT. With a heat pump designed in-house, every aspect of the VCC can be controlled including compressor speed, EXV opening, fan speeds, and power supplied to the unit. Once designed, it is recommended to conduct performance tests in a psychrometric chamber to accurately model the system. A heat pump that is controllable and easily modified increases the number of disturbances that can be studied. Lastly, the air-to-air heat pump used during experimentation is not applicable in deep space applications. Future investigations should focus on refrigerant selection and radiation-to-air heat pump components.

APPENDIX. MINI-SPLIT OPERATING PROCEDURE

A. Software Setup

- 1 Open "Mini Split" folder located on desktop
- 2 Open "ModbusClient.slx" file
- 3 While loading up, open black cabinet and turn flip all power switches on
- 4 Make sure 2020b is selected on Speedgoat display
- 5 Assure TargetPC1 is connected

B. Precheck

- 1 Check for any possible leaks around the mini-split unit
- 2 Check for any tools/materials around the unit that can cause a hazard

C. Mini-split Startup

- 1 Flip breaker handle "up" to supply power to mini-split
- 2 Turn on low voltage power supply
- 3 Check if pressure transducers and mass flow meter are on

D. Operation

- 1 Run the "ModbusClient.slx" simulink file
- 2 Check for connection (RS-485 light blinking, Gateway blinking, connection state = 1)
- 3 Input the test conditions required for desired test
- 4 Turn on unit via Simulink model ON/OFF switch
- 5 Acquire necessary data for the experiment

E. Shutdown

- 1 Turn off unit via Simulink model ON/OFF switch
- 2 Ensure pressures have equalized
- 3 Stop the Simulink simulation
- 4 Shut off power supply and flip breaker "down" to power off mini-split

REFERENCES

- [1] J. Constantinide and H. Najafi, "Present State and Future Of Environmental Control Systems In Space," *ASHRAE Journal*, vol. 62, pp. 12-16, 2020.
- [2] S. J. Dyke, K. Marais, I. Bilionis, J. Werfel and R. Malla, "Strategies for the design and operation of resilient extraterrestrial habitats," in *SPIE Smart Structures + Nondestructive Evaluation Conference*, 2021.
- [3] R. B. Malla and K. M. Brown, "Determination of temperature variation on lunar surface and subsurface for habitat analysis and design," *Acta Astronautica*, vol. 107, pp. 196-207, 2014.
- [4] M. R. Barratt, E. S. Baker and S. L. Pool, "Hypoxia, Hypercarbia, and Atmospheric Control," in *Principles of Clinical Medicine for Space Flight*, New York, Springer, 2019, pp. 137-151.
- [5] J. Broyan, D. Welsh and S. Cady, "International Space Station Crew Quarters Ventilation and Acoustic Design Implementation," in *American Institute of Aeronautics and Astronautics*, 2010.
- [6] A. Maghareh, A. Lenjani, M. Krishnan, S. Dyke and I. Bilionis, "Role of Cyber-Physical Testing in Developing Resilient Extraterrestrial Habitats," in *17th Biennial International Conference on Engineering*, 2021.
- [7] J. Park, H. Montoya, Y. Fu, A. Maghareh, S. J. Dyke and D. Ziviani, "DEVELOPMENT OF A VIRTUAL CYBER-PHYSICAL TESTBED FOR RESILIENT EXTRATERRESTRIAL HABITATS," in *Thermal and Fluids Analysis Workshop*, 2021.
- [8] M. K. Ewert, P. A. Petete and J. Dzenitis, "Active Thermal Control Systems for Lunar and Martian Exploration," *SAE International*, vol. 99, pp. 613-623, 1990.
- [9] K. R. Sridhar, M. Gottmann and A. Nanjundan, "THERMAL CONTROL SYSTEMS FOR LOW-TEMPERATURE HEAT REJECTION ON A LUNAR BASE," NASA, 1993.
- [10] R. P. Scaringe, L. R. Grzyll, G. S. Cole and J. M. Gottschlich, "Development of Heat Pump Loop Thermal Control System for Manned Spacecraft Habitats," *SAE Transactions*, vol. 111, pp. 297-304, 2002.

- [11] G. S. Cole, R. P. Scaringe, L. R. Grzyll and M. K. Ewert, "Development of a Gravity-Insensitive Heat Pump for Lunar Applications," in *Space Technology and Applications*, Albuquerque, 2006.
- [12] L. P. M. Brendel, "VAPOR COMPRESSION REFRIGERATION IN MICROGRAVITY," Purdue University Graduate School, 2021.
- [13] G. Ellis, "Model Development and Verification," in *Control System Design Guide*, Fourth ed., Butterworth-Heinemann, 2012, pp. 261-282.
- [14] Z. DU, X. JIN, Y. ZHU, Y. WANG, W. ZHANG and Z. CHEN, "Development and application of hardware-in-the-loop simulation for the HVAC systems," *Science and Technology for the Built Environment*, vol. 25, pp. 1482-1493, 2019.
- [15] P. Conti, C. Bartoli, A. Franco and D. Testi, "Experimental Analysis of an Air Heat Pump for Heating Service Using a "Hardware-In-The-Loop" System," *Energies*, vol. 13 (17), pp. 4498-, 2020.
- [16] L. Frison, M. Kleinstuck and P. Engelmann, "Model-predictive control for testing energy flexible heat pump operation within a Hardware-in-the-Loop setting," *Journal of Physics: Conference Series*, vol. 1343, 2019.
- [17] W. El-Baz, L. Mayerhofer, P. Tzscheutschler and U. Wagner, "Hardware in the Loop Real-Time Simulation for Heating Systems: Model Validation and Dynamics Analysis," *Energies*, vol. 11, pp. 3159-, 2018.
- [18] S. Wang and Z. Ma, "Supervisory and Optimal Control of Building HVAC Systems: A Review," *HVAC&R RESEARCH*, vol. 14, pp. 3-32, 2008.
- [19] Z. Afroz, G. Shafiullah, T. Urmee and G. Higgins, "Modeling techniques used in building HVAC control systems: A review," *Renewable and Sustainable Energy Reviews*, vol. 83, pp. 64-84, 2018.
- [20] MATLAB, 9.9.0.2037887 (R2020b) Update 8, Natick, Massachusetts: The MathWorks Inc., 2020.
- [21] I. H. Bell, J. Wronski, S. Quoilin and V. Lemort, "Pure and Pseudo-pure Fluid Thermophysical Property Evaluation and the Open-Source Thermophysical Property Library CoolProp," *Industrial & Engineering Chemistry Research*, vol. 53, pp. 2498-2508, 2014.

- [22] I. H. Bell, "Air conditioning and heat pump model (achp) source code version 1.5," 2015. [Online]. [Accessed 28 January 2023].
- [23] T. L. Bergman, A. S. Lavine, F. P. Incropera and D. P. Dewitt, *Fundamentals of Heat and Mass Transfer*, 7th ed., John Wiley & Sons, 2011.
- [24] J. E. Braun, S. A. Klein and J. W. Mitchell, "Effectiveness Models for Cooling Towers and Cooling Coils," in *ASHRAE Annual Meeting*, Vancouver, 1989.
- [25] M. Mihailović, U. Milovančević, S. Genić, B. Jaćimović, M. Otović and P. Kolendić, "Air side heat transfer coefficient in plate finned tube heat exchangers," *EXPERIMENTAL HEAT TRANSFER*, vol. 33, pp. 388-399, 2020.
- [26] M. M. Shah, "A New Correlation For Heat Transfer During Boiling Flow Through Pipes," *ASHRAE Transactions*, vol. 82, pp. 66-86, 1976.
- [27] Air-Conditioning, Heating, & Refrigeration Institute, "Standard for Performance Rating of Positive Displacement Refrigerant Compressors," AHRI, Arlington, 2020.
- [28] C. K. Rice and A. E. Dabiri, "A COMPRESSOR SIMULATION MODEL WITH CORRECTIONS FOR THE LEVEL OF SUCTION GAS SUPERHEAT," *ASHRAE Transactions*, vol. 87, 1981.
- [29] M. M. Shah, "A General Correlation For Heat Transfer During Film Condensation Inside Pipes," *International Journal of Heat and Mass Transfer*, vol. 22, pp. 547-556, 1979.
- [30] J. W. Mitchell and J. E. Braun, "Vapor Compression Refrigeration and Air-Conditioning Systems," in *Principles of Heating, Ventilation, and Air Conditioning in Buildings*, Wiley, 2013, pp. 401-432.
- [31] Perle, *IOLAN Secure User's Guide V5.0*, Ontario, 2022.
- [32] D. Foster and S. Ganesh, "Development of an API for Transferring Data to the Computational Subsystem within the Cyber-Physical Testbed," Resilient Extraterrestrial Habitat Institute, 2022.
- [33] L. C. Carballude, "Modeling and Experimental Validation of a Resilient Extraterrestrial Habitat Interior Environment," Purdue University Graduate School, 2023.
- [34] ASHRAE, "NONRESIDENTIAL COOLING AND HEATING LOAD CALCULATIONS," in *ASHRAE HANDBOOK - FUNDAMENTALS*, Atlanta, 2017, pp. 18.1-18.66.

- [35] H. Benaroya and L. Bernold, "Engineering of lunar bases," *Acta Astronautica*, vol. 62, pp. 277-299, 2008.
- [36] *Modular Coupled Virtual Testbed (Version 6)*, 2022.
- [37] S. W. Churchill and H. H. Chu, "Correlating equations for laminar and turbulent free convection from a vertical plate," *International Journal of Heat and Mass Transfer*, no. 18, p. 1323–1329, 1975.